The variable nature of convection in the tropics and subtropics: A legacy of 16 years of the Tropical Rainfall Measuring Mission satellite

Robert A. Houze Jr.[1], Kristen L. Rasmussen[2], Manuel D. Zuluaga[3], and Stella R. Brodzik[1]

[1]Department of Atmospheric Sciences, University of Washington, Seattle, Washington, USA, [2]Now at National Center for Atmospheric Research, Boulder, Colorado, USA, [3]Now at Universidad Nacional de Colombia, Medellín, Colombia

Abstract For over 16 years, the Precipitation Radar of the Tropical Rainfall Measuring Mission (TRMM) satellite detected the three-dimensional structure of significantly precipitating clouds in the tropics and subtropics. This paper reviews and synthesizes studies using the TRMM radar data to present a global picture of the variation of convection throughout low latitudes. The multiyear data set shows convection varying not only in amount but also in its very nature across the oceans, continents, islands, and mountain ranges of the tropics and subtropics. Shallow isolated raining clouds are overwhelmingly an oceanic phenomenon. Extremely deep and intense convective elements occur almost exclusively over land. Upscale growth of convection into mesoscale systems takes a variety of forms. Oceanic cloud systems generally have less intense embedded convection but can form very wide stratiform regions. Continental mesoscale systems often have more intense embedded convection. Some of the most intense convective cells and mesoscale systems occur near the great mountain ranges of low latitudes. The Maritime Continent and Amazonia exhibit convective clouds with maritime characteristics although they are partially or wholly land. Convective systems containing broad stratiform areas manifest most strongly over oceans. The stratiform precipitation occurs in various forms. Often it occurs as quasi-uniform precipitation with strong melting layers connected with intense convection. In monsoons and the Intertropical Convergence Zone, it takes the form of closely packed weak convective elements. Where fronts extend into the subtropics, broad stratiform regions are larger and have lower and sloping melting layers related to the baroclinic origin of the precipitation.

1. Introduction

The Tropical Rainfall Measuring Mission (TRMM) satellite launched and maintained bilaterally by the United States and Japan from 1997 through 2014 was novel in providing the first quantitative precipitation radar in space. The TRMM Precipitation Radar (PR) was deployed on the satellite together with passive microwave, visible, infrared, and lightning sensors [*Kummerow et al.*, 1998]. TRMM has provided a legacy data set of 16 years of nearly uninterrupted measurements covering the tropics and subtropics. Although the satellite was in space for nearly 17 years, the data were too preliminary in the early months and in a state of change as the satellite left its orbit in the later months. So we have restricted our assessment of the data to the 16 years of high-quality data collected between the beginning and ending months of the mission. The satellite's primary goal was to provide the climate science community with comprehensive precipitation measurement in high spatial resolution over the entire low-latitude belt, where the majority of Earth's rainfall occurs [*Simpson et al.*, 1988; *Kummerow et al.*, 2000]. Because most of the low latitudes are ocean, where surface precipitation gauges are absent, this rain pattern was only approximately known prior to TRMM. *Adler et al.* [2000] and *Huffman et al.* [2007] have described how the TRMM sensor data have been mixed with other satellite data to produce detailed rain maps and real-time prediction products, which can now be browsed online (http://trmm.gsfc.nasa.gov/). This detailed rain mapping constitutes a major success of U.S.-Japan collaboration, which continues with the successful launching of the Global Precipitation Measurement (GPM) satellite in 2014 [*Hou et al.*, 2014]. GPM now extends radar coverage into extratropical latitudes, albeit with less frequent orbital visitation.

Surface rainfall mapping was not the only goal of TRMM. The early planners of TRMM [*Simpson et al.*, 1988] realized, from work such as that of *Hartmann et al.* [1984], that knowledge of the vertical distribution of latent heating was a key to understanding the large-scale tropical general circulation and climate, and they

understood that a spaceborne radar could be used to determine the vertical distribution of latent heating accompanying the horizontal distribution of rainfall. Making simple assumptions about the vertical distribution of heating associated with the convective and stratiform components of the rainfall observed by the TRMM radar, *Schumacher et al*. [2004] calculated the impact of spatially varying latent heating profiles on the general circulation of the tropics. Similar approaches (developed by *Tao et al*. [2001, 2006, 2007, 2010, 2015] and *Shige et al*. [2004, 2007, 2008, 2009]) now use look-up tables based on more realistic models of convection to routinely produce latent heating profiles across the tropics (TRMM products 2H25 and 2H31, see the Glossary at the end of this paper for these and other acronyms). These latent heating products are providing new insight into seasonal and intraseasonal variability of the tropical circulation [e.g., *Zuluaga et al*., 2010; *Liu et al*., 2015; *Barnes et al*., 2015].

In addition to determining surface rain patterns and latent heating profiles, the TRMM three-dimensional radar data have helped to yield information on the very nature of convection. This outcome was never officially stated as a goal of TRMM [see *Simpson et al*., 1988; *Kummerow et al*., 1998, 2000], not because it was overlooked as a possibility but because it may have seemed too ambitious considering that TRMM was expected to be in orbit for ~3 years, which would not be long enough to gather a sufficiently sizable sample to parse into meaningful subsamples. Happily, TRMM remained in orbit long enough to produce a rich 16 year sample of radar data on all forms of precipitating clouds in the tropics and subtropics. As a result, TRMM has provided and continues to provide, retrospectively, considerable insight into the variable nature of convection across these latitudes.

The reasons that information on the nature of convection is obtainable from TRMM are that the PR (1) was an active sensor that collected high-resolution information on the vertical structure of radar echoes as well as on their horizontal patterns and (2) was paired with other instruments aboard the satellite. Most of the studies that have investigated the nature of convection using TRMM have approached the problem by identifying specific phenomena (or objects) satisfying certain criteria in the satellite measurements. *Nesbitt et al*. [2000] and *Toracinta et al*. [2002] identified precipitation features satisfying certain areal and intensity criteria in the PR data and associated them with the simultaneous passive microwave sensor measurements, especially those in the frequencies associated with ice scattering. They found that convection over tropical land-masses is characterized by more lightning, stronger ice scattering, and more intense radar echo in the upper levels of convective clouds than precipitating clouds over tropical oceans. *Liu et al*. [2008] developed a multi-sensor scheme to identify and characterize radar echoes seen by the TRMM PR by locating precipitation areas, cataloging their sizes and intensities, and associating them with passive microwave and lightning measurements. A database built on the *Liu et al*. [2008] scheme has led to results showing where warm rain cells occur [*Liu and Zipser*, 2009], the diurnal cycle of convection [*Liu and Zipser*, 2008; *Liu et al*., 2010], the precipitation amounts associated with rain areas of various sizes [*Liu*, 2011], the lightning characteristics of the precipitation features seen by radar [*Liu et al*., 2012], and patterns of latent heat release over the tropics [*Liu et al*., 2015].

The above studies using TRMM PR data to provide insights into the nature of convection relate TRMM echo features of a variety of sizes to certain ancillary factors derived contemporaneously from other sensors. However, it is well known that the three-dimensional structure of the precipitation field as seen by radar provides insight into the life cycle state, dynamics, and mesoscale organization of convective clouds. Simultaneous examination of the vertical as well as horizontal structure is required. Several studies have focused on the vertical structures seen by the PR. *Liu and Zipser* [2005] and *Zipser et al*. [2006] used TRMM PR data to show where the deepest convective echoes occur over the tropics and subtropics. *Boccippio et al*. [2005] examined not just echo top heights; they compiled statistics on the entire vertical profile of reflectivity seen by the TRMM PR. Using cluster analysis, they grouped the echo profiles into categories but did not associate these categories with horizontal structures. *Hence and Houze* [2011, 2012a, 2012b] compiled statistics on the histograms of radar reflectivity as a function of height in eyewall and rainbands of tropical cyclones. These studies of the vertical distributions of radar reflectivity have led to further insights but have not taken full advantage of the PR's ability to simultaneously observe both the horizontal and vertical structures of radar echoes.

In this paper, we present results gained from a methodology that carries the analysis of radar echo structures seen by the TRMM PR further by combining the TRMM PR's observations of both the horizontal and vertical

structures of radar echoes into a single algorithmic approach. By doing so a wide range of convective behavior across the tropics and subtropics is revealed. The smallest, shallowest rainclouds, the deepest and most intense convective cells, convection growing upscale into mesoscale units, and mesoscale systems producing large regions of stratiform rain can all be distinguished using this methodology. Applying this method to the whole of the region covered by TRMM we can determine where each of these convective features manifests most strongly as well as where they do not exist or develop. Because the convective behaviors identified relate to convective life cycle stage, we are able to distinguish regions where clouds do and do not become especially deep and/or intense, where they do and do not aggregate into mesoscale systems, and where mesoscale systems do and do not produce great regions of stratiform precipitation as an adjunct to the deep convection. This methodology is thus useful for studies of the geographical and climatological variability of convective life cycle behavior, which must ultimately be represented accurately in regional and global models.

We first used this methodology to study convection over the Indian subcontinent [*Houze et al.*, 2007; *Romatschke et al.*, 2010]. These studies showed a striking contrast between the nature of convection in the arid region of Pakistan and northwestern India and the wetlands of Bangladesh and the Indian state of Bengal. This work was an early indication of the power of the PR data to show fundamental differences in the nature of convection from one region to another. We also applied the methodology to South America and Africa [*Romatschke and Houze*, 2010; *Rasmussen and Houze*, 2011; *Rasmussen et al.*, 2014; *Zuluaga and Houze*, 2015] and found clear distinctions between precipitating convection over the Pampas of subtropical South America and the tropical region of Amazonia. We also found a striking similarity of convection over equatorial Africa and portions of South America, and vast differences between convection over land and ocean in these regions. Applying this method to PR data obtained over the Indian Ocean and West Pacific showed how the nature of precipitating convection is related to the changing large-scale environment during passages of the Madden-Julian Oscillation [*Barnes and Houze*, 2013; *Barnes et al.*, 2015].

This methodology is demanding to apply, and up to now we have concentrated on applying it in regional studies. However, the rich variability in the nature of convection seen in these regional studies inspires a global examination of this variability over the entire tropics and subtropics. This motivation has led to the present paper in which we apply the methodology over the entire zone covered by the TRMM orbit to determine how the different forms of convection vary across the entire tropical and subtropical zone. In this way, we aim to evaluate more comprehensively the forms taken by convective clouds throughout the heated portion of Earth's atmosphere. It is especially fitting to attempt such a global evaluation as numerical models of the general circulation rapidly increase in resolution and detail, especially insofar as they represent clouds and precipitation. Understanding how the nature of precipitating convective clouds varies around the globe, from oceans to dry lands, to wetlands, to forests, to mountains, will be the basis for determining whether global models accurately represent how the nature of convection varies from one region of Earth to another.

2. Methodology

The methodology that we use to combine vertical and horizontal structural information from the TRMM PR identifies and characterizes precipitating cloud elements according to their heights, widths, intensity, and stratiform versus convective character. We begin with the archived TRMM data products 2A25, which provides the field of radar reflectivity, and 2A23, which separates the radar echoes into convective and stratiform components [*Awaka et al.*, 1997]. For completeness, the 2A23 product identifies categories that are called "other" because they cannot be easily distinguished as convective or stratiform. These other echoes are a small fraction of the total echo population. *Schumacher and Houze* [2003a] found that they accounted for $< 0.2\%$ of rainfall observed by the TRMM PR. *Funk et al.* [2013] counted the number of pixels classified as other in later revisions of the TRMM PR data set and found that if noise and artifacts are included $< 2\%$ is classified as other and that if only precipitation echoes were considered $< 0.2\%$ was flagged as other. The 2A23 product also subdivides the convective echoes into various shallow and deep categories. Our methodology extends this technique by seeking additional subcategories of convective and stratiform echoes by applying threshold metrics for their height, breadth, and intensity. From these subcategories of convective and stratiform radar echoes, we are able to objectively recognize different forms of convection over the tropics and subtropics.

Our methodology is distinct in that it makes full use of the vertical structure of radar echoes observed by the TRMM PR. To examine the vertical structure nimbly, we have reprocessed the TRMM PR data recorded along radar beams by geolocating all of the attenuation corrected radar reflectivity data archived in bins located along the slant range of the radar beam and archived as part of TRMM product 2A25 and interpolating them onto a Cartesian grid. The three-dimensional geolocated and interpolated radar reflectivity data set and all of the derived products described in this paper are available at trmm.atmos.washington.edu. It is this three-dimensional Cartesian gridded data set that allows us to apply our algorithmic approach to distinguish the internal structures of the convective elements seen by TRMM in a way that relates the echoes to the probable life cycle stage, intensity, and degree of mesoscale organization of the convective clouds.

Houze et al. [2007] describe the basic idea of the geolocation and interpolation methodology. The code has been rewritten and made more efficient over the years, but the basic idea is the same. *Houze et al.* [2007] also introduced the basic procedure for identifying certain types of radar echoes via their three-dimensional structure determined from the Cartesian gridded data. In our past studies for specific regions of the tropics and subtropics, we have used two different forms of the method for identifying types of echoes from their three-dimensional structure. The difference in the forms is that one form uses a set of "strong" thresholds that better represent the behavior of convection over land, while the other form uses a set of "moderate" thresholds that better exhibits convective behavior over oceans (see *Barnes and Houze* [2013] for further discussion of the use of these threshold sets over ocean versus land). Since we analyze convective structures over the whole of the tropics and subtropics in this paper, and because we wish to see how results vary smoothly over the globe, we do not presuppose our results by choosing one or the other threshold set depending on location. Rather, we apply both sets of thresholds at every location in the latitude belt regardless of the underlying surface. Thus, we compare two sets of results throughout the paper, one using the strong thresholds and the other using the moderate thresholds. This approach accommodates the fact that some land surface areas, such as Amazonia, behave somewhat like oceanic convection, while areas that are a mix of land and ocean, such as the Maritime Continent, are not well represented by either of the threshold sets alone.

Before the thresholds are applied, the entire TRMM PR data set from 1998 to 2013 is scanned to locate every distinguishable rain area (DRA) defined as consisting of two or more contiguous pixels containing detectable radar echoes. It should be noted that in 2001, the orbital altitude was boosted from 350 to 402 km, which changed the PR pixel size from 4.3 to about 5 km [*Short and Nakamura*, 2010]. This change had no noticeable effect on the type of analysis reported here. Any areas containing isolated pixels are ignored. We do not use data from 2014 because during that year the satellite was undergoing maneuvers related to its decommissioning. After all DRAs are identified, they are subjected to further analysis to identify four subcategories of convective echo and one subcategory of stratiform echo.

One subcategory of DRA that we use in this study is isolated shallow echoes (ISEs): These echoes are a standard subcategory identified by the TRMM 2A23 product and were analyzed over the tropics in an earlier study by *Schumacher and Houze* [2003b]. They are precipitating elements whose echo tops are at least 1 km below the 0°C level and may be thought of as showers of "warm rain."

The ISEs represent the smallest end of the precipitating convective cloud spectrum. To represent the larger and most intense of the convective entities, we examine all DRAs in the whole 16 year data set to determine if the DRA contains certain types of embedded echo objects. For every DRA, we determine if it contains a three-dimensional contiguous volume of echo flagged by 2A23 as convective that exceeds a given threshold intensity (strong threshold 40 dBZ; moderate threshold 30 dBZ). This procedure is computationally intensive because the archived data must first be regridded onto a Cartesian coordinate frame to make these determinations [see *Houze et al.*, 2007]. Once all embedded echo features exceeding the strong or moderate threshold are identified, we determine the horizontal and vertical dimensions of these high-intensity embedded convective echo objects. Using these dimensions, we identify the following two types of intense embedded convective echoes:

1. *Deep convective cores* (*DCCs*). DCCs are defined as those contiguous three-dimensional convective echo objects exceeding either the moderate or strong threshold intensity whose tops exceed a height threshold. For echo objects defined by the moderate threshold intensity of 30 dBZ, the echo objects' top-height threshold is 8 km to qualify as a DCC; for the strong threshold intensity of 40 dBZ, the height threshold is 10 km. Whether defined by the moderate or strong thresholds, DCCs are associated with young, vigorous convection.

2. *Wide convective cores* (*WCCs*). These three-dimensional echo volumes represent extremely intense convection that has organized upscale into mesoscale units exhibiting high reflectivity. WCCs are defined as those contiguous 3-D convective echo objects exceeding either the moderate or strong threshold intensity whose horizontal dimensions (at some altitude) exceed a given threshold. For echo objects defined by the moderate threshold intensity of 30 dBZ, the echo objects' horizontal area threshold size is 800 km^2; for the strong threshold intensity of 40 dBZ, the area threshold is 1000 km^2.

The ISEs, DCCs, and WCCs represent three different extrema of convective behavior. By trial and error, we have found that the 30 and 40 dBZ thresholds applied in three dimensions for ocean and land conditions, respectively, represent well the most intense end of the convective spectrum. Because WCCs have no height criterion, they are not a subset of DCCs nor are DCCs a subset of WCCs. However, the two categories have some overlap; some three-dimensional echo objects satisfy both DCC and WCC thresholds. We keep track of the three-dimensional echo objects that satisfy both DCC and WCC conditions. This hybrid category accounts for about 10% of the number of WCCs found over land regions, and analyses show that this category behaves in all respects in a manner intermediate between the DCC and WCC categories [e.g., see *Zuluaga and Houze*, 2013, 2015; *Rasmussen et al.*, 2014]. Therefore, we do not include discussion of the combined deep and wide category in the present paper.

We also examine every DRA to determine if it contains an extreme form of stratiform precipitation—Broad stratiform regions (BSRs): A large region of convectively initiated stratiform precipitation is a manifestation of a mature and very well developed mesoscale convective system [*Houze*, 2004]. To signify such a feature, a broad stratiform region is defined as a contiguous stratiform echo (as designated by the 2A23 product) covering at least 40,000 km^2 (moderate threshold) or 50,000 km^2 (strong threshold). We examine every DRA to determine if it contains a BSR.

It is important to realize that a DCC or WCC is of such a high reflectivity that it is always part of a larger cloud system; they are never entities unto themselves. We therefore may speak of a clouds or "storms" containing a DCC or WCC. Similarly, a BSR may be part of a parent mesoscale system that has coexisting convective rain elements within the same cloud system. Some BSRs existing at an instant late in a cloud system's lifetime might comprise a single echo with no adjoining convective features. Nonetheless, it would be part of a cloud system that had active convection earlier in its lifetime. TRMM PR data represent snapshots and cannot track the histories of the echoes containing DCCs, WCCs, or BSRs. Mesoscale convective systems exhibit a wide range of lifetimes. For example, *Chen et al.* [1996] found lifetimes of ~2–20 h over the tropical West Pacific. By tracking echoes observed by ground-based radar, and applying the same criteria that we use for DCCs, WCCs, and BSRs in TRMM satellite data, *Zuluaga and Houze* [2013] confirmed statistically that DCCs, WCCs, and BSRs are almost always features of the early, middle, and late stages of mesoscale convective systems, and they will be regarded as such in the following sections of this paper.

3. Rainfall in the Tropics and Subtropics as Seen by the TRMM PR

The rain maps in Figure 1 show the average rain rate across the tropics and subtropics as seen by the PR for two seasons: boreal winter/austral summer, represented by December-January-February (DJF); and boreal summer/austral winter, represented by June-July-August (JJA) over the 16 years of data. If a pixel lies within a DRA, then its rain rate is assumed to be given by the TRMM 2A25 near-surface rain product. The mean rain rate at a given location is determined by summing all of the rain rates recorded by 2A25 when a DRA is over the pixel defining that location and then dividing that sum by the number of overpasses of the TRMM PR during the time period under consideration. An important point regarding the rain maps is that the TRMM orbit extends to latitudes of about 35°. As a result, during the winter seasons, the rain seen at the northern and southern borders of Figures 1a and 1b, respectively, is due in part to extratropical frontal systems and is therefore not comparable in causation to the precipitation of convective origin in the remainder of the tropical and subtropical zone. The frontal precipitation at the higher latitudes of the TRMM orbital swath is most pronounced in the winter hemispheres. This different nature of the precipitation between equatorial and subtropical latitudes will be important in some of the physical interpretations offered in the sections below.

To demonstrate how important storms containing extreme echo elements of the types described above (DCC, WCC, and BSR) are to the total rainfall in the tropics and subtropics, Figure 2 shows mean rain rate due to storms that do not contain such echoes. Figures 2a and 2c (Figures 2b and 2d) show the mean rain
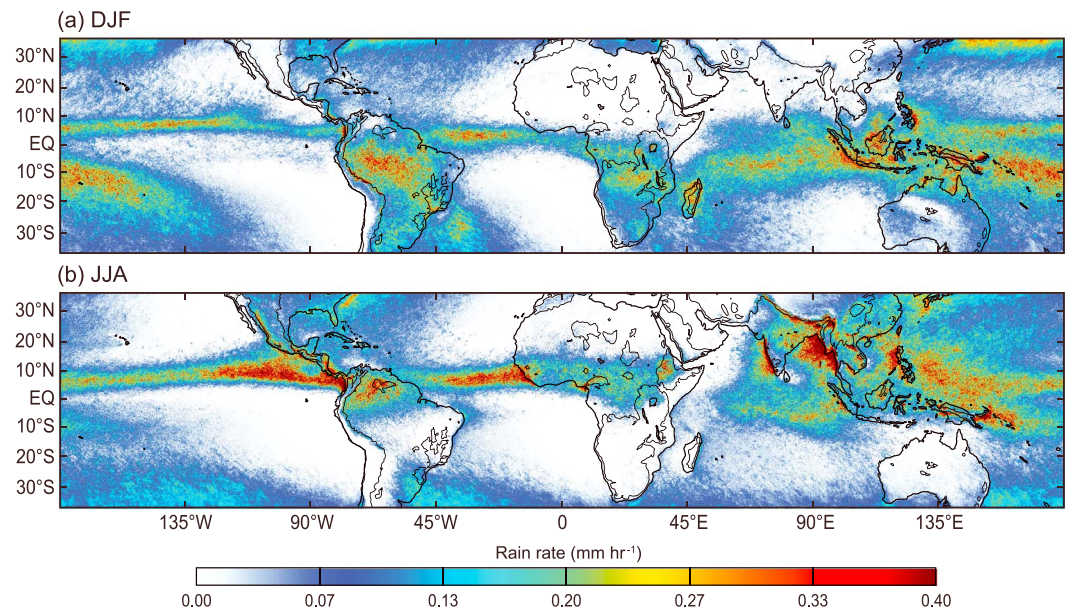
Figure 1. Precipitation climatology expressed in average rain rates (mm h^{-1}) from all TRMM Distinguishable Rain Areas (DRAs) during the months of (a) DJF and (b) JJA from 1998 to 2013. The black contour inside the continental regions represents the 700 m elevation.

rates due to storms not containing echo elements defined by the strong (moderate) thresholds. Comparison of Figures 1 and 2 shows that over nearly all of the tropics and subtropics, storms not containing DCCs, WCCs, and BSRs account for only a small residual of the rainfall, whether defined by strong or moderate thresholds. One notable exception is apparent just upstream of the mountainous western coasts of India and Burma during JJA. In the predominant low-level southwesterlies of the summer monsoon, these zones have a substantial amount of rain falling from storms that do not contain extreme echoes defined by the strong thresholds (Figure 2c). If the moderate threshold set is used to define DCCs, WCCs, and BSRs, then even these monsoonal coastlines do not have much rain from storms not containing embedded echoes of these extreme types. We nevertheless conclude that the monsoonal rains in these regions are the result of a different, less extreme type of convection than in other regions of the tropics and subtropics. This fact will also be notable in the analyses of the patterns of DCCs, WCCs, and BSRs presented in the remainder of this paper.

4. Extremely Shallow and Deep Convection

We begin by comparing the patterns of occurrence of the shallowest and deepest forms of convection. Figure 3 shows (a and b) the frequency of occurrence of ISEs for each analyzed season and (c and d) the frequency of DCCs (using strong thresholds over the entire tropics and subtropics). The frequency is presented as a probability on a scale of 0 to 1 and is computed as the number of pixels identified as belonging to an echo category divided by the total number of pixels sampled by the TRMM PR over the given time period within a 0.5° × 0.5° grid element. (Note color scales vary from panel to panel and from similar panels in other Figures.) Further discussion of the probability calculation is in Appendix A of *Romatschke et al.* [2010]. The DCCs using strong thresholds are the most robust manifestation of convection, computed with the intensity threshold of 40 dBZ and height threshold of 10 km. Figures 3b and 3d show that the penetration of a 40 dBZ echo to a height of 10 km or greater almost never occurs over the ocean and occurs over land only in the locations pointed out by *Zipser et al.* [2006]: the southeastern U.S., Argentina (especially close to the Andes in summer), near-equatorial Africa and America, and northwest India and Pakistan (close to the intersection of the Himalayas and mountains of Afghanistan). In contrast, ISEs occur almost exclusively over the warm oceans and practically never over land (Figures 3a and 3c).

The ISEs and extreme DCCs are opposite both in their nature and in their locations of occurrence. This behavior is easy to understand. It is well known from elementary cloud physics that the large salt particles and low concentrations of aerosol over oceans make small-to-moderate cumulus clouds efficient at quickly forming
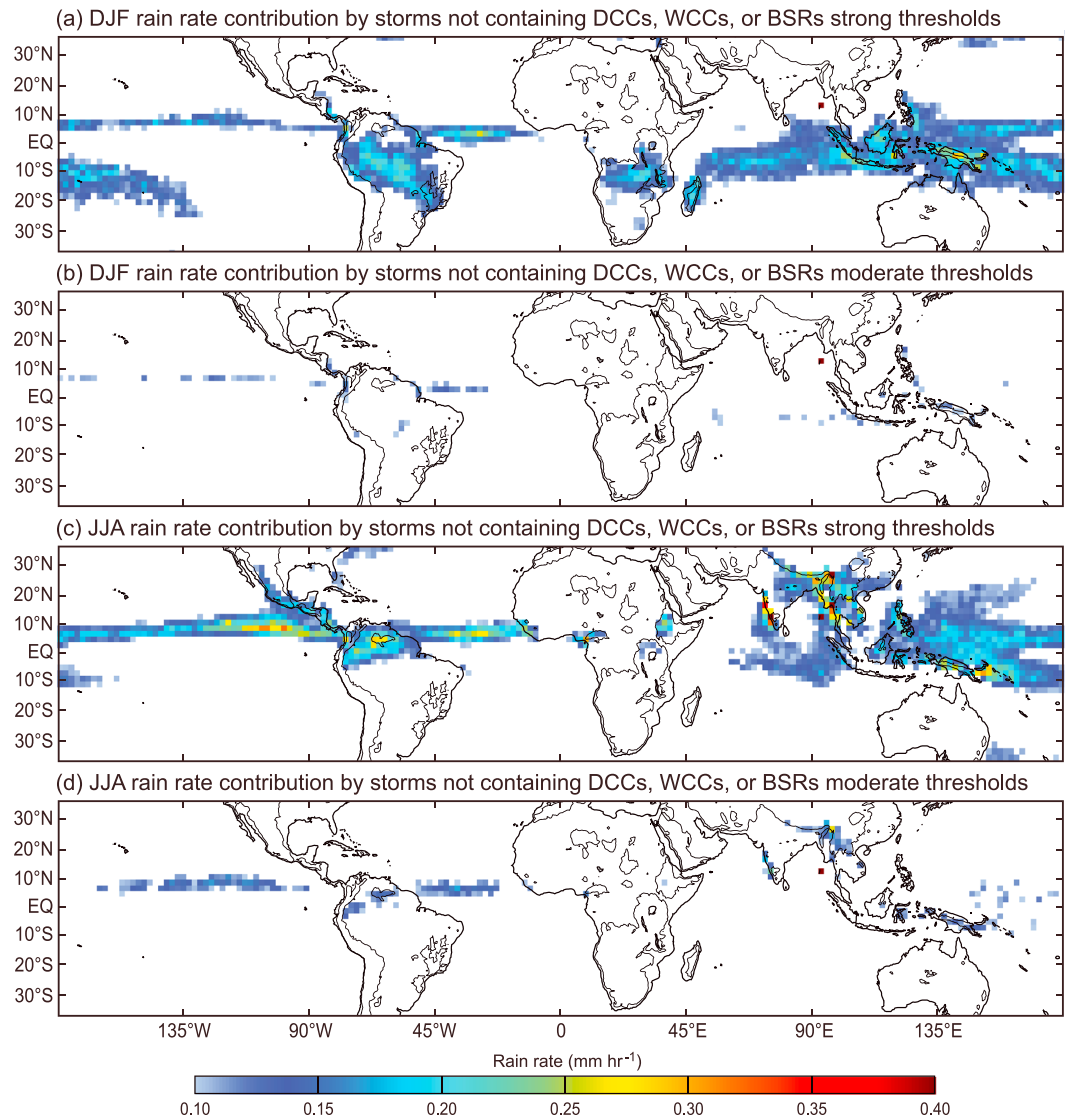
Figure 2. Residual climatological precipitation rain rates (mm h^{-1}) contributed by storms not containing DCCs, WCCs, or BSRs for the months of DJF from the (a) strong and (b) moderate thresholds, and for the months of JJA from the (c) strong and (d) moderate thresholds from TRMM PR data. Mean rain rates < 0.1 mm h^{-1} have been masked out to highlight the areas where the effects of storms not containing DCCs, WCCs, or BSRs are largest. The black contour inside the continental regions represents the 700 m elevation.

rain over tropical oceans. The opposite aerosol characteristics over land make it difficult for ISE clouds to prosper over land. On the other hand, the occurrence of nearly dry adiabatic lapse rates over land provides great buoyancy values to support the occurrence of DCCs. Over oceans, lapse rates are almost never so steep. As pointed out by *Xu and Emanuel* [1989], the tropical oceanic atmosphere is almost always close to moist adiabatic, which implies that rising parcels of air cannot deviate strongly from environmental temperature and thus seldom achieve large values of buoyancy. Note that this fact does not preclude convection from becoming deep, rather it means that while rising to high altitudes the parcels may proceed more slowly. *LeMone and Zipser* [1980] and *Zipser and LeMone* [1980] found that vertical velocities encountered by aircraft in deep convection over tropical oceans were typically much lower than over land. Occasional exceptions have been noted, especially where tropical cyclogenesis is occurring [*Zipser and Gautier*, 1978; *Houze et al.*, 2009], but statistics overwhelmingly show low vertical velocities over the oceans. The lower vertical velocities over the oceans cannot support the generation of large supercooled water concentrations required for the graupel and hail particle formation that would explain the existence of 40 dBZ echoes at heights above
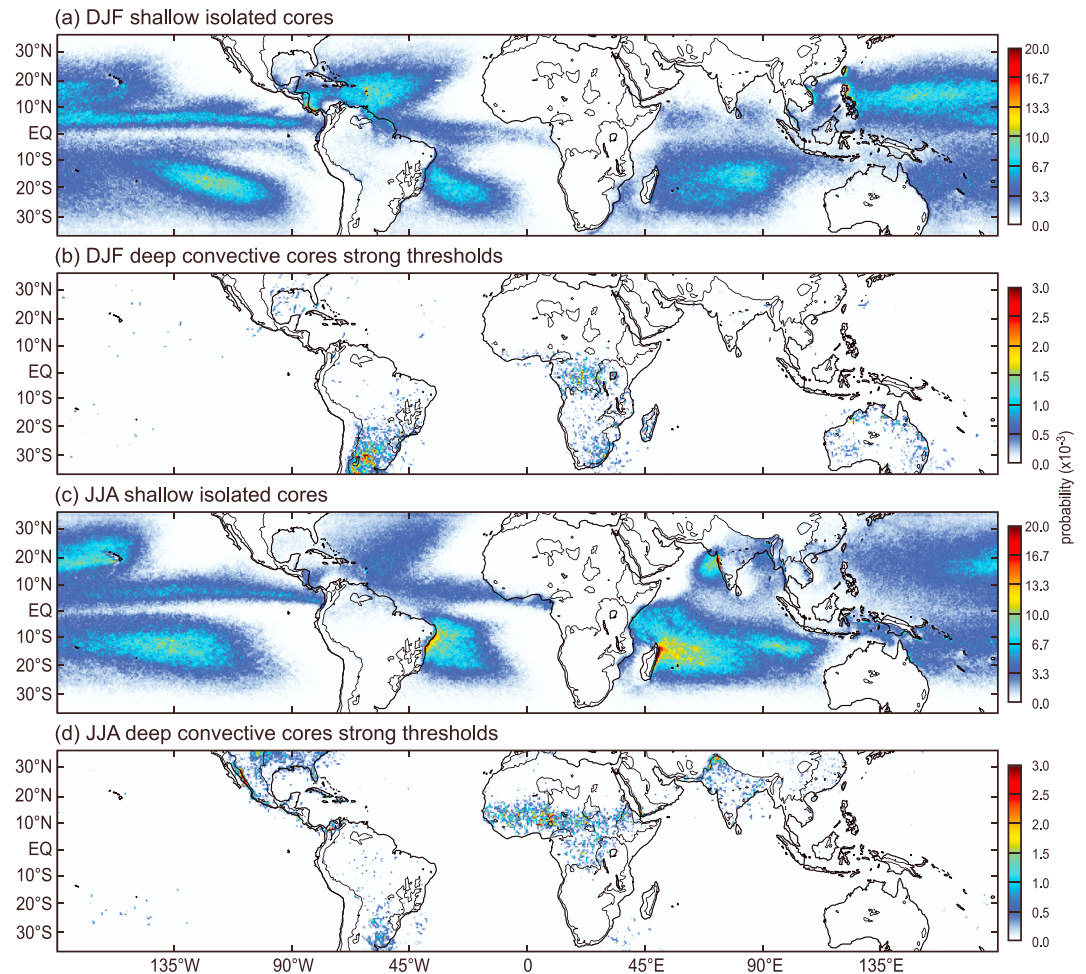
Figure 3. Geographical distribution of the probability of finding (a) ISEs and (b) strong threshold DCCs during the months of DJF, and (c) ISEs and (d) strong threshold DCCs during the months of JJA from TRMM PR data. The black contour inside the continental regions represents the 700 m elevation. The probability is on a scale of 0 to 1 and is computed as the number of pixels identified as belonging to an echo category divided by the total number of pixels sampled by the TRMM PR over the given time period within a 0.5° × 0.5° grid element.

10 km. Such high reflectivities measured at the these altitudes by the 2 cm wavelength of the TRMM PR are most likely the result of Mie scattering by particles of dimensions near or greater than the radar wavelength, and the low vertical velocities over oceans cannot produce such particles. This interpretation is further supported by the results of *Nesbitt et al.* [2000], who showed that ice scattering in the 89 GHz passive microwave channel was seen in precipitating clouds over land far more strongly than over tropical oceans, and by the results of *Barros et al.* [2004], who showed a maximum of lightning corresponding over northwestern India and Pakistan, at the location of maximum DCC frequency seen in Figure 3d (and previously pointed out by *Houze et al.* [2007]).

In JJA, high concentrations of ISE clouds occur along the coasts of South America and Madagascar, where the landmasses jut out to the east. From Figure 4, we can see how these points of land intersect the southeast trade winds so that low-level convergence tends to be maximized along and just upwind of the coasts.

5. Upscale Development of Convection

5.1. Why the Horizontal Scale of Convection Is Important

Often the size spectrum of convective clouds in the atmosphere is expressed as a function of cloud height [e.g., *Arakawa and Schubert*, 1974]. However, convective clouds vary in horizontal as well as vertical dimension. When convective elements group together a mesoscale convective system (MCS) may result. As discussed in
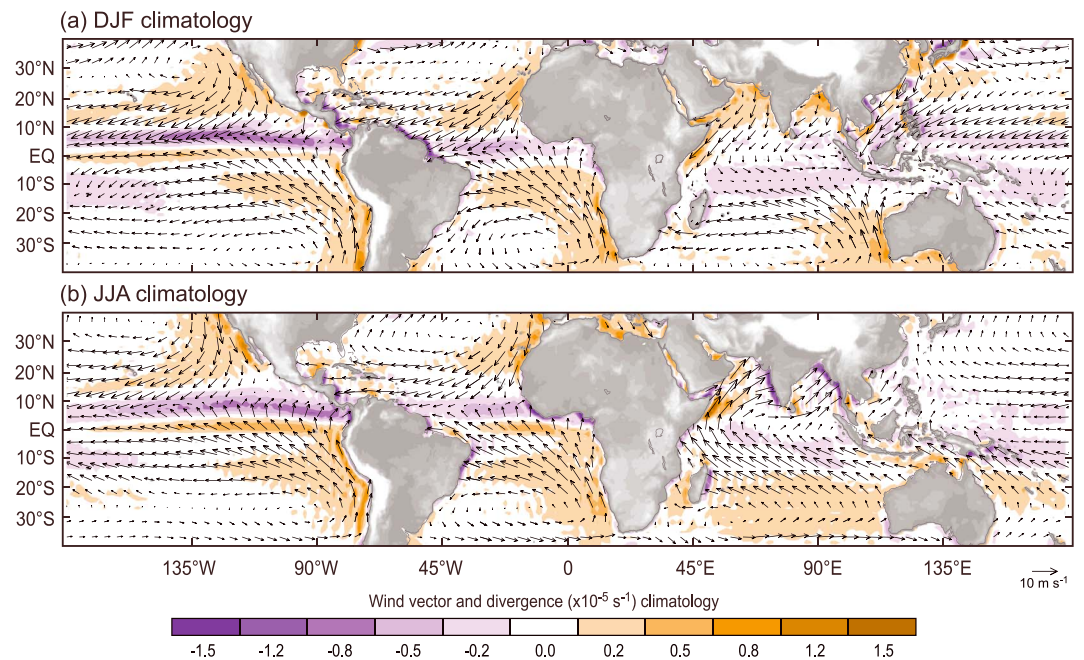
Figure 4. Climatology of 1000 hPa wind vectors and divergence ($10^{-5}\,s^{-1}$), represented by vectors and shaded contours, respectively, for the months of (a) DJF and (b) JJA. Continental data are omitted to highlight the oceanic wind patterns.

the review of *Houze* [2004] and in Chapter 9 of *Houze* [2014], an MCS develops a mesoscale overturning circulation that is dynamically distinct from that of a convective cell, which occurs on a smaller spatial scale. While a convective cell is well described by entraining parcel concepts and consists of a buoyant plume or bubbles ~1–10 km in horizontal scale originating in the boundary layer and accelerating upward, the circulation of an MCS consists of broad layers of rising and sinking air on horizontal scales ~100 km. The mesoscale layer overturning of an MCS has been described as the gravity-wave response to the collective convective heating in a group or line of convective cells [*Pandya and Durran*, 1996] or alternatively as a joint mesoscale response to the environmental thermal and wind stratifications [*Moncrieff*, 1992]. The layer of subsiding air in an MCS enters at midlevels [*Kingsmill and Houze*, 1999] and is driven downward by the cooling effects of evaporation and melting of precipitation particles below a layer of upward motion and condensation heating aloft [*Houze*, 1982, 1989]. *Fritsch et al.* [1994] showed how the heating aloft and cooling below in the stratiform region generates potential vorticity, enhancing and prolonging the MCS.

MCSs are of great importance to atmospheric dynamics and physics for several reasons. The latent heating profile in an MCS shifts upward (becomes "top heavy") when the stratiform component of the MCS is large. *Hartmann et al.* [1984] and *Schumacher et al.* [2004] have shown that accounting for the upward shift of the vertical distribution of heating leads to more realistic large-scale circulation of the tropics. MCSs are also important because they account for numerous events of excessive rainfall, severe weather, and floods [e.g., *Hoxit et al.*, 1976; *Bosart and Sanders*, 1981; *Houze et al.*, 1990; *Rasmussen and Houze*, 2011; *Romatschke and Houze*, 2013; *Rasmussen et al.*, 2014]. In addition, MCSs are the location of upper atmospheric electrical events (such as sprites) that connect the troposphere and ionosphere through the global electric circuit [*Hager et al.*, 2012]. These facts motivate a global understanding of when and where deep convection organizes upscale into mesoscale units.

Below we will examine how the methodology of identifying TRMM radar echoes defined as deep convective cores and wide convective cores indicates where upscale growth to the mesoscale occurs and from what kind of convection. To account for the seasonal shifting of patterns of convection over the globe, we will examine the two opposite seasons DJF and JJA.

5.2. Upscale Growth of Convection in DJF

As was seen in Figures 3b and 3d, DCCs defined by the strong threshold set occur almost exclusively over land. As noted in the previous section, it is well known that convection over the warm oceans is typically
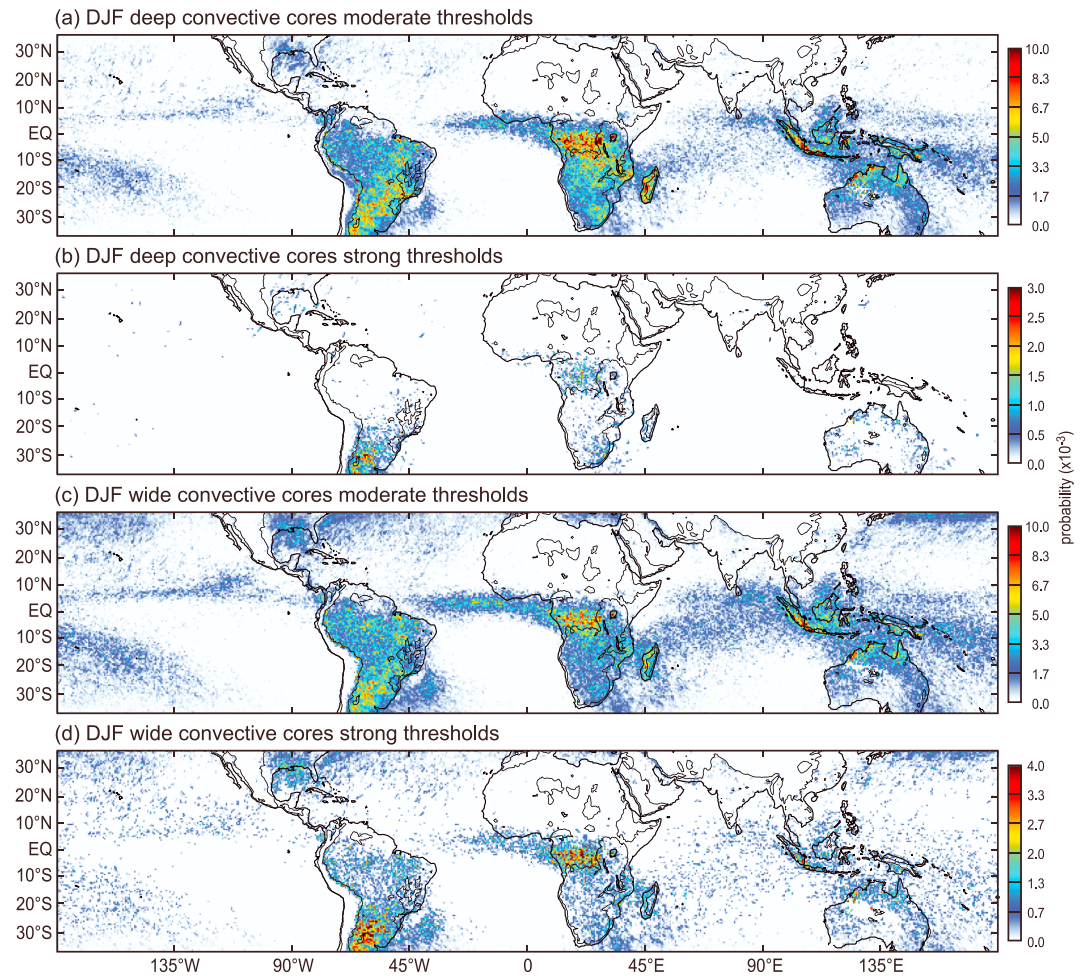
Figure 5. Geographical distribution of the probability of finding (a) DCCs with moderate thresholds, (b) DCCs with strong thresholds, (c) WCCs with moderate thresholds, and (d) WCCs with strong thresholds during the months of DJF from TRMM PR data. The black contour inside the continental regions represents the 700 m elevation. The probability is on a scale of 0 to 1 and is computed as the number of pixels identified as belonging to an echo category divided by the total number of pixels sampled by the TRMM PR over the given time period within a 0.5° × 0.5° grid element.

much less intense than over land. Figures 5a and 5b show that during the DJF season the moderate threshold set locates DCCs over broader regions than where the extreme DCCs identified by the strong threshold set occur. Comparing Figures 5a and 5b shows that the moderate DCCs are most frequent in the locations where strong DCCs are found. However, the moderate DCCs are not confined to land but occur also over the oceans, wherever rain occurs in the tropics and subtropics. Thus, we see that storms containing strong DCCs are extreme cases that do not occur everywhere tropical and subtropical precipitation occurs, but storms with moderate DCCs occur in nearly all precipitation regions in low latitudes (cf. Figures 5 and 1a).

To see where deep convection grows into mesoscale cloud systems and from what types of convective clouds, we compare the locations of WCCs shown in Figures 5c and 5d to the locations of ISEs in Figures 3a and 3c and to the locations of DCCs in Figure 5a and 5b. Comparison of the regions of frequent ISE occurrence (Figures 3a and 3c) to the favored locations of moderate WCCs over the oceans in Figure 5c is consistent with the notion of "self aggregation" of smaller convective cells into mesoscale units as advocated by *Wing and Emanuel* [2013] and *Emanuel et al.* [2014] being active over the tropical oceans. However, the absence of fields of small convective elements over the land regions suggests that mechanism may not as active over the tropical continental regions.

A more universal correspondence is seen between moderate DCCs and WCCs. Moderate WCCs occur everywhere in proportion to the occurrence of moderate DCCs. However, the same is not true for DCCs defined by

the strong threshold set; strong DCCs are infrequent in precipitation zones. Two locations especially stand out, tropical South America and the Maritime Continent. Tropical South America (especially the Amazon region) is a region of maximum rainfall in DJF (Figure 1a). Yet over tropical South America strong DCCs almost never occur (Figure 5b), whereas moderate WCCs are common over the whole Amazonian area (Figure 5c). Thus, we see that the Amazon region is the home of much upscale development of convection, but the convection leading to the upscale growth is of a relatively moderate nature. We note further that WCCs defined by the strong threshold set (Figure 5d) also occur over all of Amazonia but with much less frequency than the moderate WCCs (Figure 5c). The results in Figure 5 thus indicate that Amazonian rainfall is a result primarily of convective systems of a relatively moderate character. In this way, the patterns of occurrence of deep and wide convective cores over the Amazon region imply a convective population somewhat similar to oceanic regions. Convective behavior over the Amazon region has sometimes been likened to oceanic convection [*Romatschke and Houze*, 2010], especially under westerly flow conditions [*Cifelli et al.*, 2002]. The results presented here establish that deep convection in the region of the Amazon is strongly climatologically similar to oceanic convection.

Another zone in which the convection differs from that in other regions is the Maritime Continent (Indonesia, Malaysia, and Northern Australia). When *Ramage* [1968] dubbed this region the "Maritime continent," he pointed out that its geographical uniqueness, heavy rainfall, and powerful diurnal cycle were unlike any other location on Earth. Indeed, he pointed out, the Maritime Continent at this time of year is the locus of more rain and hence latent heat release than anywhere else on Earth. This region is actually neither continental nor maritime but rather is an archipelago consisting of large islands and peninsulas separated by wide yet confined straits. The statistics of DCCs and WCCs exhibit a behavior similar to the Amazon region. Despite having the highest tropopause in the atmosphere, the Maritime continent region has virtually no strong DCCs (Figure 5b). However, it is densely populated with moderate DCCs and moderate WCCs (Figures 5a and 5c, respectively). Like the Amazon region, the Maritime Continent is characterized by upscale growth of moderate convection to form numerous moderate mesoscale systems. Some strong WCCs occur in the region (Figure 5d), but the moderate systems dominate. Thus, the Amazon and Maritime Continent, two of the rainiest places in the world (Figure 1), are dominated by moderate deep convection growing upscale into moderate mesoscale precipitating cloud systems.

We note further from Figures 5a and 5b that during DJF the convective behavior over the southeast coast of the U.S. is muted due to wintertime conditions, with an absence of strong DCCs but a presence of a few cloud systems with moderate DCCs, which are probably connected with frontal systems extending southward into the region. Figures 5c and 5d show that WCCs defined by both moderate and strong thresholds also appear in the region of the southeastern U.S. but are probably more associated with frontal forcing than upscale growth of convection.

Figure 5d shows that in DJF (austral summer), WCCs signaling the areas of upscale growth of convection into the strongest of mesoscale systems occur in two notable areas: equatorial Africa and subtropical South America (mainly Argentina). These two areas are also the two areas where strong DCCs are most concentrated (Figure 5b). These statistics indicate that storms containing the deepest and most intense convective cells tend to grow upscale into mesoscale systems containing the widest and most intense convection.

5.3. Upscale Growth of Convection in JJA

Some of the convective behaviors seen in DJF are also evident in JJA, with patterns shifting toward the Northern Hemisphere. Figure 6 indicates the following behaviors that are similar to DJF.

1. Strong DCCs occur only over land.
2. Moderate DCCs and moderate WCCs occur both over land and ocean and are seen wherever tropical and subtropical rain occurs.
3. Northern South America and the Maritime Continent have an absence of strong DCCs but a profusion of moderate DCCs and WCCs, indicating that two of the rainiest regions on Earth are dominated by storms with moderately deep convection growing upscale into moderately mesoscale systems and not by the deepest and most intense storms.

One area exhibiting unique characteristics in boreal summer is the region of Mesoamerica: the Gulf coast of the U.S., Cuba, and Hispaniola. This region has a pronounced pattern of moderate DCC occurrence. Figure 7a
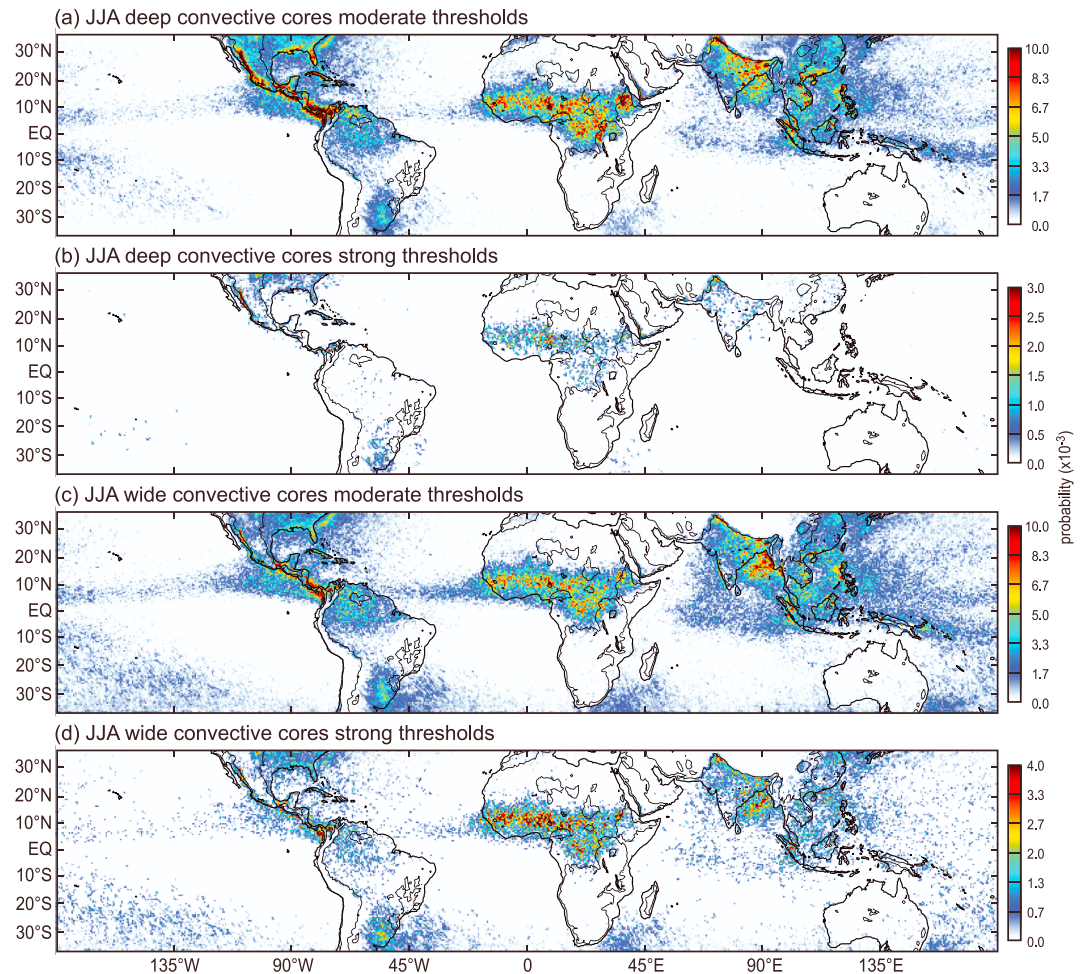
Figure 6. Same as in Figure 5 but for the months of JJA.

zooms in on this portion of Figure 6a. Figure 6b further shows that these processes seldom produce strong DCCs except along a narrow line atop the Sierra Madre Occidental of Mexico. Narrow zones of high frequency of moderate DCCs occur near coastlines.

The zones of DCC occurrence seen in Figure 7a correspond to where diurnal sea-land-mountain forcing is known to trigger convection. Sometimes the zones are over near-coastal mountain ridges, especially over the near-coastal high terrain of the Sierra Madre Occidental, a region where diurnal convection was the focus of the North American Monsoon Experiment (NAME) [*Higgins et al.*, 2006]. Using dual-polarimetric radar data obtained in NAME, *Rowe et al.* [2008, 2011, 2012] examined the microphysics and dynamics of the storms containing diurnally forced deep convective cells. Sometimes the maxima in Figure 7 are offshore, the result of land breeze triggering. Over the Florida peninsula, which is nonmountainous, the maximum of DCC occurrence is over the land, where the deep convective cells form in response to sea breezes from both the Atlantic and Gulf of Mexico [*Burpee and Lahiff*, 1984]. The diurnal convection over Florida has been the subject of many field studies, the most extensive of which was the Convection and Precipitation/Electrification Experiment (CaPE; summaries of the experiment can be found at http://weather.msfc.nasa.gov/irgrp/cape. html and http://opensky.library.ucar.edu/collections/SOARS-000-000-000-292). *Yuter and Houze* [1995a, 1995b, 1995c] used dual-Polarimetric radar data from CaPE to examine the microphysics, vertical velocity, and mass transport by these convective cells. Over Colombia, in the northwestern corner of South America, the moderate DCCs manifest over the lower slopes and foothills of the northern extension of the Andes and over the Gulf of Panama off the Colombian Coast. *Zuluaga and Houze* [2015] examined the behavior of this convection with respect to the diurnal cycle and the larger-scale circulation in this region.
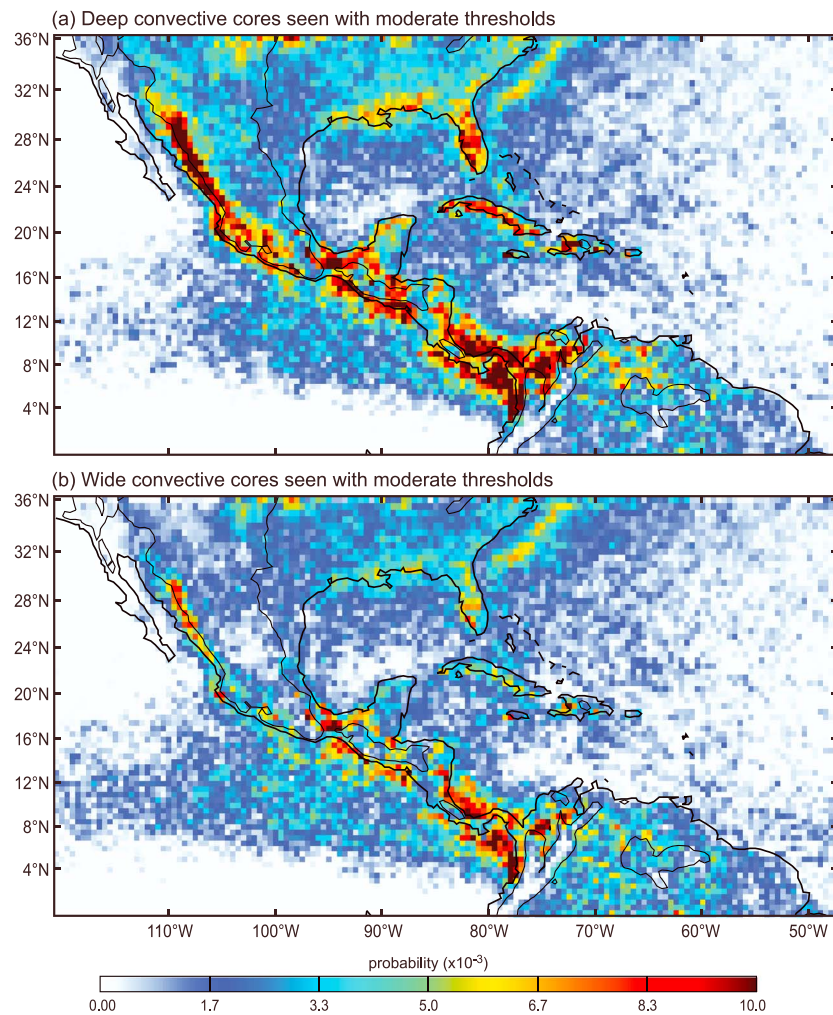
Figure 7. Geographical distribution of the probability of finding (a) DCCs with moderate thresholds and (b) WCCs with moderate thresholds over the Mesoamerica region. Figures 7a and 7b are zoomed-in portions of Figures 5a and 5c, respectively, over Mesoamerica. The black contour inside the continental regions represents the 700 m elevation. The probability is on a scale of 0 to 1 and is computed as the number of pixels identified as belonging to an echo category divided by the total number of pixels sampled by the TRMM PR over the given time period within a $0.5° \times 0.5°$ grid element.

The moderate and occasionally strong convective cells forming in the regions shown in Figures 6a and 7a frequently amalgamate and grow upscale to form mesoscale systems within which WCCs occur. Figure 6b and the zoomed-in Figure 7b show that the DCCs in the Mesoamerican and Gulf-Caribbean regions frequently grow upscale to form mesoscale systems containing moderate and occasionally strong WCCs. Such mesoscale systems have been analyzed in detail by *Rowe et al.* [2008, 2011, 2012], *Yuter and Houze* [1995a, 1995b, 1995c], and *Zuluaga and Houze* [2015].

Another convective manifestation seen in JJA that is not present in DJF is the deep and wide convection associated with the South Asian summer monsoon. To better see results over South Asia, Figure 8 zooms in on that portion of Figure 6. The patterns of occurrence of storms with DCCs, WCCs, and BSRs in the South Asian monsoon have been presented in detail by *Houze et al.* [2007] and *Romatschke et al.* [2010]. These previous studies have shown that DCCs defined by the strong threshold occur frequently over Pakistan and Northwest India, in the crook formed by the Himalayas and mountains of Afghanistan. Figure 8c bears out this result. *Zipser et al.* [2006] pointed out that the extremely intense deep convection in this region is comparable to that over Argentina in the austral summer in being some of the deepest convection in the world. The reason for the occurrence of strong DCCs in this region is the influx of low-level moist warm air from the Arabian Sea and capping of the moist layer by downslope flow from the Afghan Plateau until
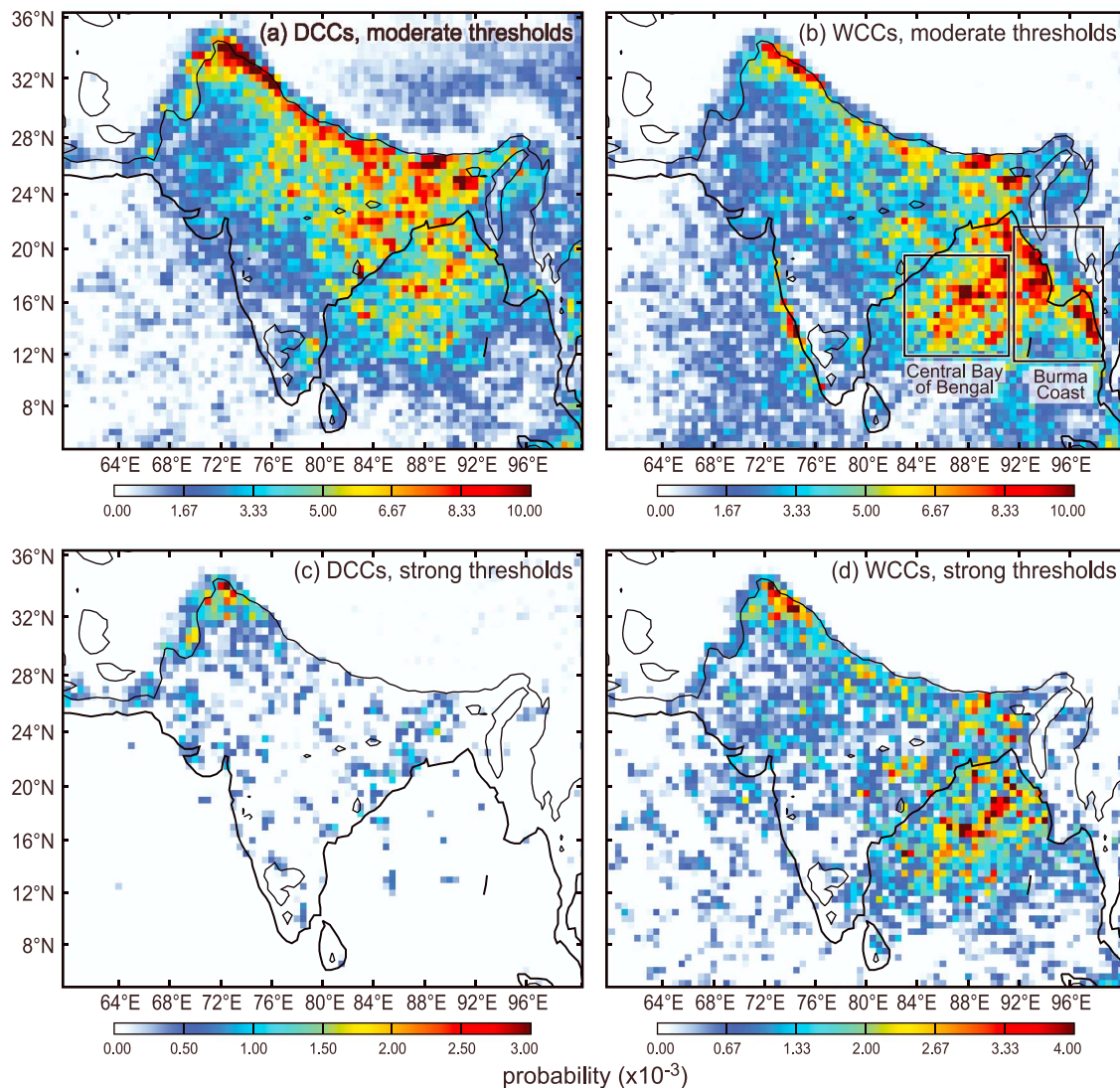
Figure 8. Geographical distribution of the probability of finding (a) DCCs with moderate thresholds, (b) WCCs with moderate thresholds, (c) DCCs with strong thresholds, and (d) WCCs with strong thresholds during the months of JJA over Southeast Asia. Figures 8a–8d are zoomed-in portions of Figure 5 over Southeast Asia. The black contour inside the continental regions represents the 700 m elevation. The probability is on a scale of 0 to 1 and is computed as the number of pixels identified as belonging to an echo category divided by the total number of pixels sampled by the TRMM PR over the given time period within a 0.5° × 0.5° grid element. Statistics for the rectangular regions are given in Table 1. Examples of the structures of BSRs occurring in the rectangular regions are shown in subsequent figures and discussed in the text.

convection is released by orographic lifting over the foothills of the great mountain ranges [*Sawyer*, 1947; *Houze et al.*, 2007; *Medina et al.*, 2010]. However, comparison of Figures 8a and 8c shows that away from this unique zone, the DCCs in South Asia are mostly those defined by the moderate threshold set. The moderate DCCs occur all along the Himalayan foothills and are generally widespread over eastern India and the Bay of Bengal. This pattern of moderate DCCs corresponds to the area frequented by Bay of Bengal depressions during active periods of the South Asian monsoon [*Ramage*, 1971; *Krishnamurti et al.*, 1975; *Rao*, 1976; *Godbole*, 1977; *Sikka*, 1977; *Shukla*, 1978; *Sanders*, 1984; *Johnson and Houze*, 1987; *Douglas*, 1992a, 1992b; *Houze et al.*, 2007].

The similarity of patterns in Figures 8a, 8b, and 8d indicates that the convective systems with moderate DCCs over eastern India and the Bay of Bengal frequently grow upscale into mesoscale systems containing WCCs. Such mesoscale systems were one focus of the Global Atmospheric Research Program's Summer Monsoon Experiment of 1979 [*Krishnamurti*, 1985; *Houze and Churchill*, 1987]. Comparison of Figures 8b and 8d shows a subtle but important difference in the patterns of occurrence of moderate and strong WCCs. In addition to the maximum of occurrence of moderate WCC radar echoes in the middle of the Bay of Bengal, further

maxima are tightly connected to the coastline of Burma on the eastern edge of the Bay. This pattern suggests the existence of two types of mesoscale cloud systems. The type in the center of the Bay would be conventionally associated with upscale growth of cloud systems containing the DCCs that occur there. However, Figure 8a shows relatively few occurrences of DCCs along the coast of Burma. The WCCs hugging the coastline in Figure 8b may grow upscale from amalgamations of shallower but heavily raining convective cells (not qualifying even as moderate DCCs), or such WCCs may be an effect of the southwesterly monsoon flow impinging on the mountains of Burma and enhancing the precipitation processes just upstream of the barrier. These two types of mesoscale systems are described in more detail later in section 7.2.

6. Convectively Generated Large Stratiform Precipitation Areas

Schumacher and Houze [2003a], *Nesbitt and Anders* [2009], *Biasutti et al.* [2012], and others have described the general breakdown of tropical and subtropical rain into generally stratiform and convective components, as shown by the TRMM PR. As discussed by *Houze* [1997], the stratiform rain areas are composed of hydrometeors originating in areas of more active convection. In this section and section 7, we investigate the occurrence and structures of the most extreme stratiform areas—the BSRs, which are stratiform rain echoes extending contiguously over extremely large areas. By noting where these echoes occur in relation to deep convection and by examining their vertical structure, we see that these extremely large stratiform regions take on different forms in different regions of the tropics and subtropics, and that they do not all appear to be of the type of stratiform structure associated with MCSs of the type reviewed by *Houze* [2004].

6.1. WCCs and BSRs Do Not Maximize in the Same Places

A BSR often can often be interpreted as an indicator of a later stage mesoscale system of the type described by *Houze* [2004]. The idea is that DCCs and WCCs occur when convective systems are growing upscale. In WCCs, several intense convective elements are packed close together on the mesoscale. A well developed mesoscale convective system can produce a large region of stratiform precipitation as deep convection ages and/or by the winds aloft shearing the system into a highly tilted mode [*Houze*, 2004, 2014]. One of the important features of the TRMM radar is that it shows where precipitation connected with tropical convection exhibits stratiform characteristics. In previous papers focusing on South America, *Romatschke and Houze* [2010] and *Rasmussen and Houze* [2011] found it informative to determine where the largest regions of convectively generated stratiform rain (BSRs) occur in relation to the preferred locations of deep and wide convective cores (DCCs and WCCs). These comparisons showed that the storms with BSRs were systematically downstream of storms containing WCCs, and that the latter storms were downstream of storms with DCCs, indicating a systematic life cycle behavior. This behavior was very evident in South America but is not universal over the tropics and subtropics.

Figure 9 is not restricted to a particular region, and from it we can compare the patterns of occurrence of WCCs and BSRs in all regions of the tropics and subtropics. BSRs occur in all regions where storms with WCCs occur. However, these coincident occurrences exhibit region differences between land and ocean. The primary regions of occurrence of BSRs over land are in southern South America (Argentina) in DJF and near-equatorial Africa in both DJF and JJA. Although BSRs occur in those continental regions, these regions are not the locations of most frequent BSR occurrence. The greatest frequencies of BSR occurrence are over the oceans. WCCs occur in all of the oceanic regions of maximum BSR occurrence. However, the WCCs are not especially frequent in the oceanic zones of high occurrence of BSRs except along the west coasts of tropical Africa and South America. Thus, WCCs manifest most strongly over land, with a moderate occurrence of BSRs in the same locations, while BSRs manifest most strongly over oceans with less obvious coincident occurrence of WCCs.

6.2. Regions of Frequent BSR Occurrence

Because WCC and BSR occurrence patterns in Figure 9 suggest that the relationship between convection containing WCCs and BSRs varies from one region to another, the next section of the paper will examine the vertical structures of the radar echoes occurring in several of the regions of most frequent BSR occurrence. The rectangles in Figure 10 show the locations where we will focus our examination. The colors of the rectangles indicate regions that exhibit certain types of radar echo structure. The red rectangles are adjacent to the west coasts of landmasses in monsoonal regions and extending in the major oceans westward into the Intertropical Convergence Zone (ITCZ). The blue rectangles are over regions of the West
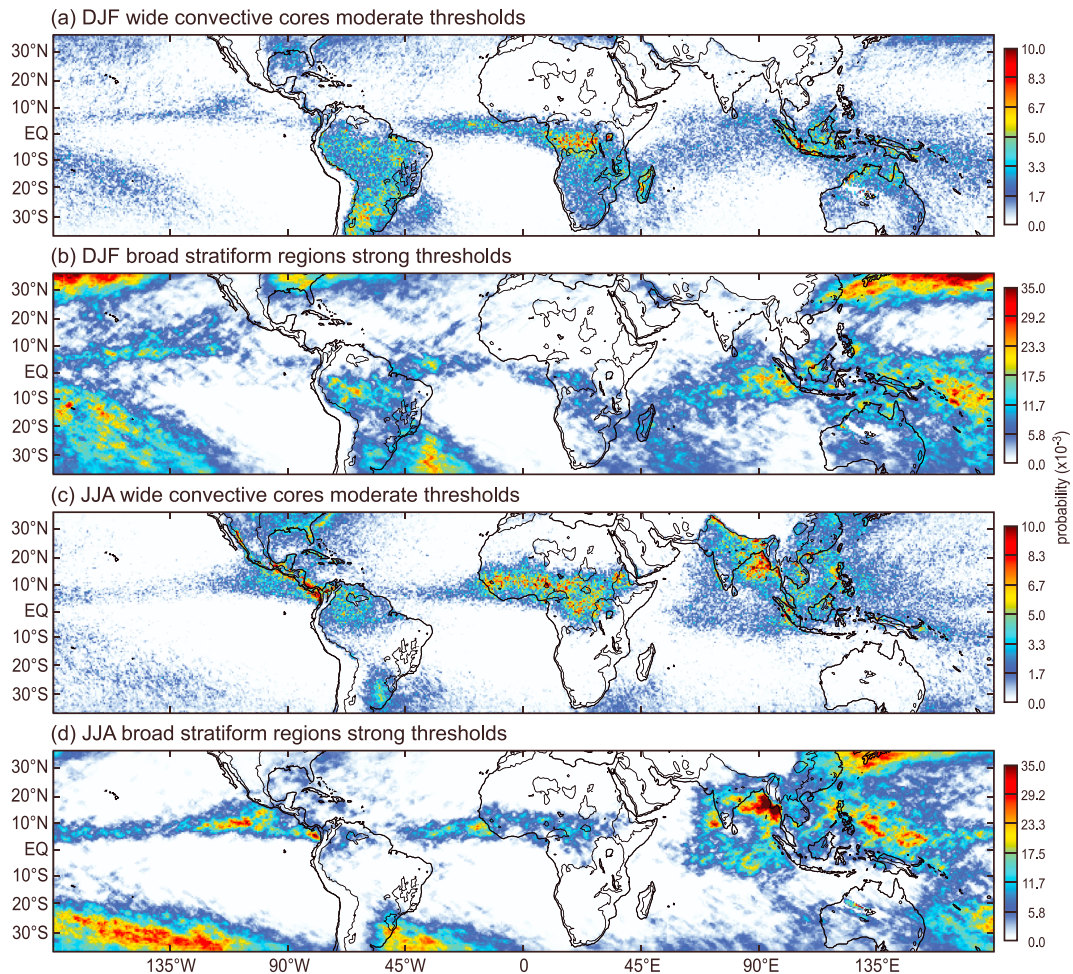
Figure 9. Geographical distribution of the probability of finding (a) WCCs with moderate thresholds and (b) BSRs with strong thresholds during the months of DJF, and (c) WCCs with moderate thresholds and (d) BSRs with strong thresholds during the months of JJA. The black contour inside the continental regions represents the 700 m elevation. The probability is on a scale of 0 to 1 and is computed as the number of pixels identified as belonging to an echo category divided by the total number of pixels sampled by the TRMM PR over the given time period within a $0.5° \times 0.5°$ grid element.

Pacific warm pool. The green rectangles are located along the meridional boundaries of the subtropics during winter seasons. These regions reflect the wintertime equatorward extent of midlatitude frontal systems, and the cloud systems in these regions may therefore be fundamentally of a different nature than those nearer the equator. The orange rectangle is unique; it is located in the region affected by the summertime Mei-Yu front convergence, where southwesterly low-level flow around the North Pacific subtropical high meets air flowing off the eastern Asian continent. The next section examines the vertical structures of the BSRs that occur in these different regions of the tropics and subtropics.

7. Vertical Structures of Stratiform Regions

As noted in section 2, our methodology is based on a Cartesian gridded version of the TRMM PR data set. The Cartesian gridded data facilitate the use of software such as the Mountain Zebra software developed at the National Center for Atmospheric Research [*Corbet et al.*, 1994] and modified at the University of Washington [*James et al.*, 2000] to accommodate the presence of underlying complex terrain. This software allows us to manually and quickly examine the data in arbitrary user-selected cross sections. Restricting analysis to a set of fixed *x* and *y* coordinates in other types of analysis tools makes the analysis of vertical structure slow and difficult. With this more nimble approach, we have examined thousands of cross sections. In the following subsections, we summarize our findings obtained by showing examples of the application of our cross-section methodology to the BSRs occurring in the regions identified by the rectangles in Figure 10.
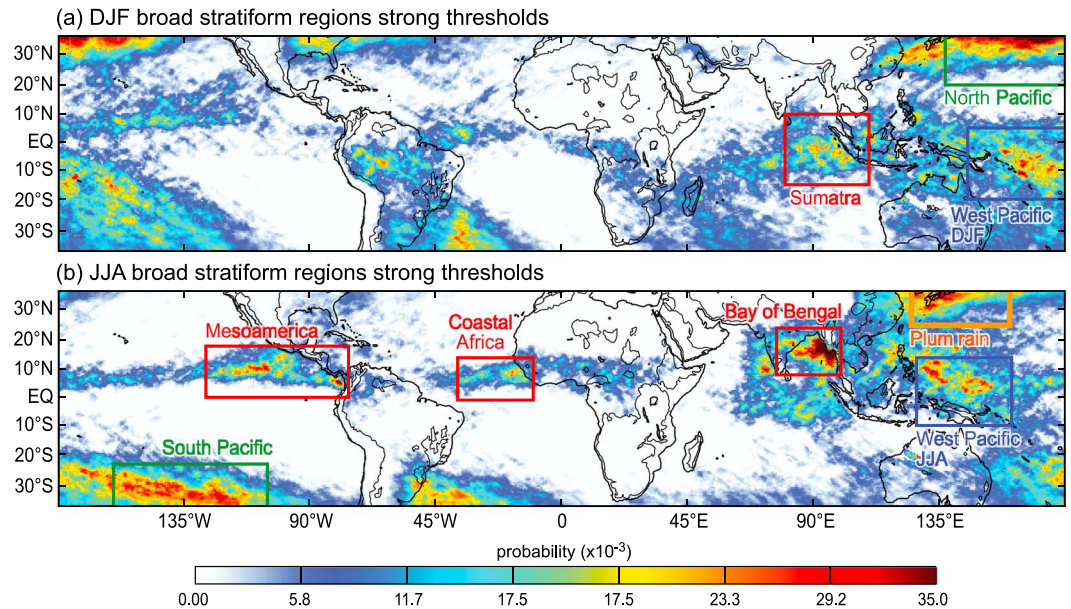
Figure 10. Geographical distribution of the probability of finding (a) BSRs with strong thresholds during the months of DJF and (b) BSRs with strong thresholds during the months of JJA. The colored rectangles indicate regions of interest discussed in sections 6.2 and detailed in Figures 11–15. The rectangles outline regions selected to represent the warm pool region (blue), monsoonal regions (red), the "plum rain" region (orange), and frontal zones (green). The probability is on a scale of 0 to 1 and is computed as the number of pixels identified as belonging to an echo category divided by the total number of pixels sampled by the TRMM PR over the given time period within a 0.5° × 0.5° grid element.

7.1. Warm Pool Regions

The West Pacific "warm pool" is a region known for its large MCSs, the largest of which was dubbed "superclusters" by *Nakazawa* [1988] and *Mapes and Houze* [1993]. In the Tropical Ocean Global Atmosphere Coupled Ocean Atmosphere Response Experiment (TOGA COARE), the large MCSs in this region were documented in great detail by airborne and shipborne Doppler radar [e.g., *Chen et al.*, 1996; *Rickenbach and Rutledge*, 1998; *DeMott and Rutledge*, 1998; *Kingsmill and Houze*, 1999; *Houze et al.*, 2000]. The largest MCSs reported in these studies were notable not only for their great size but also for their especially large regions of stratiform precipitation [e.g., *Chen et al.*, 1996; *Houze et al.*, 2000]. The frequent occurrence of BSRs seen by TRMM in this region is therefore not surprising. Several hundred BSRs in the blue rectangle regions of Figure 10 were examined using the Mountain Zebra software, and Figure 11 shows vertical cross sections of their typical vertical structures. As in the TOGA COARE storms, stratiform regions with strong bright bands extended over wide areas. The bright bands often exceeded 35 dBZ and frequently were more than 40 dBZ in intensity, indicating the melting of large snow particles from deep widespread stratiform cloud in the middle-to-upper troposphere. Examples from TRMM BSRs are shown in Figures 11a–11d. The case in Figure 11a illustrates the typical well-formed stratiform regions that are usually found in the vicinity of very deep and intense convective echoes in this region. We will refer in the remainder of the paper to stratiform regions with such strong coherent extensive bright bands as "robust." Figures 11b and 11c show robust stratiform regions extending over distances ~400 km. These large intense stratiform regions occur in both JJA and DJF.

The example in Figure 11d is different. The precipitation area contains numerous elements that were small in horizontal scale and interconnected by very weak radar echo. This whole weak echo region of irregular texture is identified as stratiform by the TRMM 2A23 algorithm and because of its large contiguous horizontal extent is flagged as a BSR. This weaker cellular-appearing BSR could be old and decaying remnants of an earlier robust BSR, or it could be a different type of stratiform precipitation feature that does not form in connection with strong deep convection but rather from the weakening of a grouping of smaller, weaker convective cells.

Table 1 contains the average sizes of BSR echoes in the regions indicated by rectangles in Figure 10. It also lists the percentages of the echoes examined that were of the weak cellular nature seen in Figure 11d.
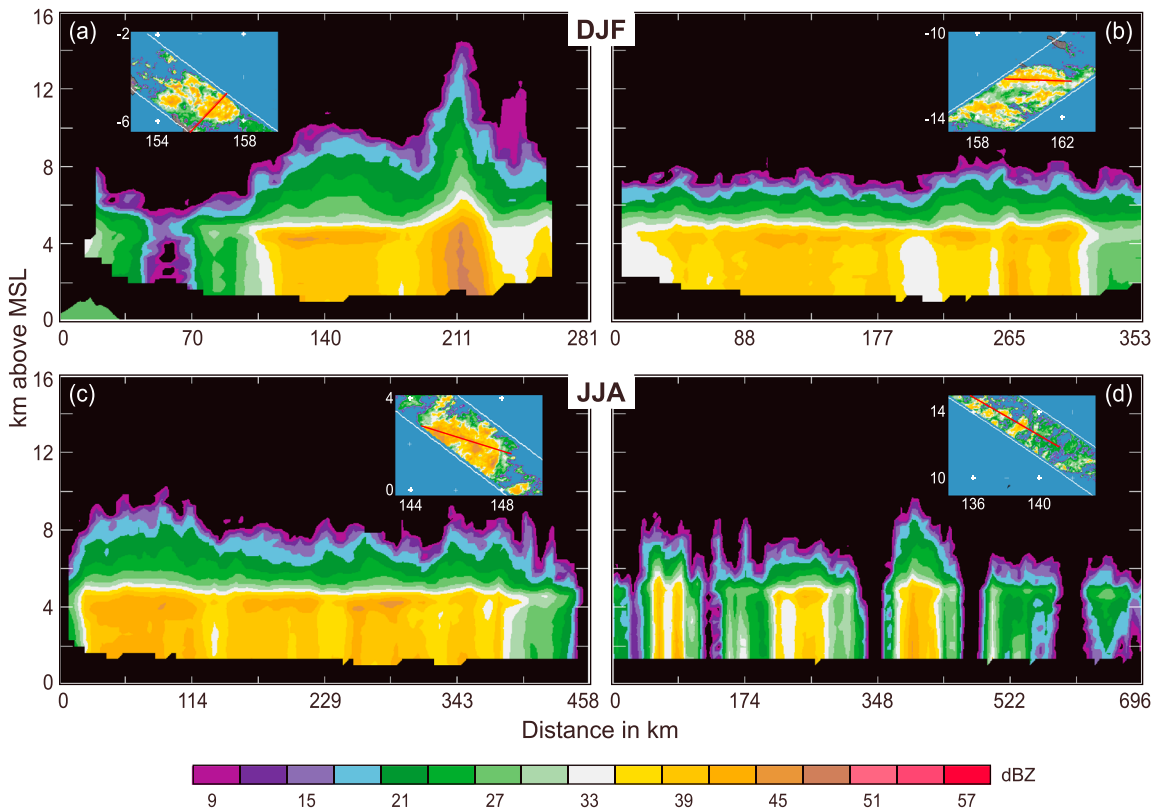
Figure 11. Examples of storms containing BSRs in the blue rectangles that represent the warm pool region in Figure 10. TRMM PR reflectivity data in dBZ at 4 km are represented by the plan view insets in Figures 11a–11d. The white lines indicate the TRMM PR swath, and the red line indicates the location of the vertical cross section from left to right. Positive latitudes are in the Northern Hemisphere. Longitudes are all in the Eastern Hemisphere. Vertical cross sections of TRMM PR data representing robust stratiform precipitation from the blue rectangle in Figure 10a, during the months of DJF, are presented at 16:18 UTC, 21 January 2010 (Figure 11a) and 16:08 UTC, 14 January 2008 (Figure 11b). Vertical cross sections of TRMM PR data representing robust stratiform precipitation and widespread cellular stratiform from the blue rectangle in Figure 10b, during the months of JJA, are presented at 00:36 UTC, 23 July 1999 (Figure 11c) and 05:26 UTC, 5 August 2009 (Figure 11d), respectively.

This type of echo is rare over the West Pacific region in JJA (12.5%) and even rarer in DJF (7.4%). However, as will be discussed below, these weaker BSRs are more common in other oceanic regions.

7.2. Monsoonal and ITCZ Convection

Figure 12 shows several examples of TRMM radar vertical cross sections through echoes identified as stratiform by the TRMM 2A23 algorithm and as BSRs by our methodology. These examples are taken from the monsoonal and ITCZ regions indicated by red rectangles in Figure 10. Two distinctly different types of echoes emerge from our comprehensive examination of hundreds of such echoes over these offshore monsoonal

Table 1. Statistics of Broad Stratiform Regions Located in the Regions Indicated in Figure 10

| Region	Average BSR Area (km^2)	Standard Deviation of BSR Area (km^2)	Robust BSRs (%)	Widespread/ Cellular BSRs (%)	Midlatitude Frontal BSRs (%)	Number of BSR Cases Examined	Total Number of BSRs
West Pacific (DJF)	75,281	25,976	88.9	7.4	-	54	294
West Pacific (JJA)	75,258	25,060	87.5	12.5	-	48	1,125
Bay of Bengal (JJA)	72,107	23,318	70.7	29.3	-	58	566
Coastal Africa (JJA)	65,184	13,761	56	44	-	50	121
Mesoamerica (JJA)	69,991	21,230	51	49	-	49	570
Sumatra (DJF)	73,367	26,145	50	50	-	50	838
Plum rain (JJA)	89,776	41,418	46.9	30.6	12.2	49	1,245
South Pacific (JJA)	85,161	38,748	-	-	79.2	48	2,270
North Pacific (DJF)	94,891	45,181	-	-	78	50	1,589
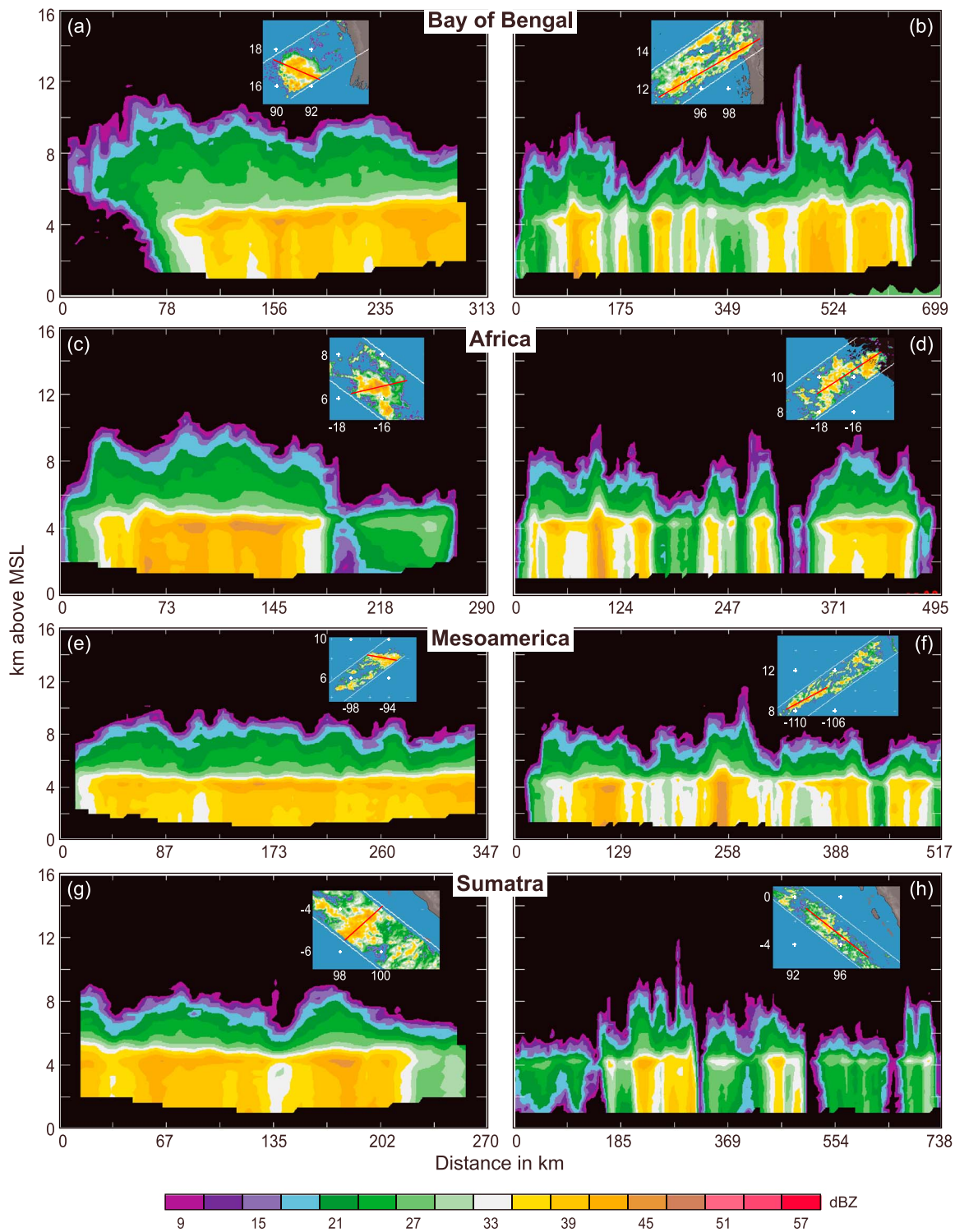
Figure 12. Same as in Figure 11 but for the red rectangles that represent the monsoonal regions shown in Figure 10. (a, c, e, and g) Vertical cross sections of TRMM PR data representing robust stratiform precipitation and (b, d, f, and h) those representing widespread cellular stratiform precipitation. Examples of TRMM PR data are provided for each of the four red rectangles shown in Figure 10: 14:01 UTC, 3 June 2003 (Figure 12a) and 21:08 UTC, 28 June 2006 (Figure 12b) from the Bay of Bengal region (JJA); 11:51 UTC, 8 June 2011 (Figure 12c) and 12:19 UTC, 30 July 2006 (Figure 12d) from the coastal Africa region (JJA); 13:44 UTC, 11 July 2011 (Figure 12e) and 04:51 UTC, 13 August 2012 (Figure 12f) from the Mesoamerica region (JJA); and 10:04 UTC, 26 February 2002 (Figure 12g) and 15:50 UTC, 27 December 2010 (Figure 12h) from the Sumatra region (DJF).

and ITCZ regions. Figures 12a, 12c, 12e, and 12g show examples of one type, which have an intense bright band across a wide region of generally moderate precipitation. We only show a few representative examples here, but in many of the TRMM PR snapshots we have investigated in vertical cross section, these wide areas of robust stratiform radar echo were in close proximity to deep convective echoes. These robust stratiform regions are readily interpreted to be the stratiform portions of mature MCSs of the type reviewed by *Houze* [2004], and as such there is no reason not to think that they have heating profiles like those assigned to them by the TRMM 2H25 and 2H31 algorithms [*Tao et al.*, 2001, 2006, 2007; *Shige et al.*, 2004, 2007]. These strong coherent stratiform regions of the mesoscale convective system type were often found well away from the coastlines.

In contrast, Figures 12b, 12d, 12f, and 12h show echoes also identified as stratiform by the 2A23 algorithm and extending over regions wide enough to be identified as BSRs by our methodology. These BSR examples have a much different appearance. They do not exhibit strong coherent bright bands but rather consist of closely spaced weak and shallow vertically oriented echoes or "cells." A faint but nearly continuous bright band extends horizontally across the region of weak cells. Evidently, in these weak cellular BSR cases convective updrafts are present but not strong enough to prevent sedimentation and melting of ice particles from forming weak bright bands; these weak bright bands evidently trigger the 2A23 algorithm to identify the region as stratiform despite the decidedly cellular nature of the reflectivity field. It is doubtful that these BSRs have heating profiles like those of mesoscale convective systems. These echoes are often but not always found near coastlines where the onshore flow meets near-coastal terrain. This tendency is most pronounced over the Bay of Bengal along the Burmese coastline. The strong maximum of BSR frequency seen in that region in Figures 9d and 10b is intensified by the presence of these broad but cellular echoes being identified as stratiform by the 2A23 algorithm. Recall that echoes identified as WCCs by moderate thresholds also maximize at the Burma coastline (Figure 8b), whereas WCCs identified by the strong threshold set are centered over the Bay of Bengal and do not cluster near the coast (Figure 8d). Our interpretation is that BSRs over the center of the Bay are associated with strong WCCs centered over the Bay, while the BSRs hugging the coast of Burma are associated with the moderate WCCs located there. The persistent southwesterly monsoonal low-level winds blowing against the Burmese near-coastal mountain terrain (Figure 4b) must favor continual upstream formation of smaller convective elements so that they pile up in this region. Such behavior would be analogous to the piling up of smaller convective elements on the coast of South America and Madagascar (Figure 3c). Sometimes the closely packed cells are strong enough to qualify as moderate WCCs (defined by a 30 dBZ threshold) and at other times, when they are weaker, the echoes do not form WCCs but rather aggregate to form radar echoes identified as BSRs. We suggest that such echoes may be falsely identified as stratiform and are unlikely to have the same kind of heating profile as applies to the robust stratiform regions seen in Figures 12a, 12c, 12e, and 12g. *Zhang et al.* [2004] found that ITCZ regions have a bimodal overturning structure. We speculate that the shallow cellular BSRs in ITCZ regions may be associated with the shallow overturning mode while the robust BSRs with wide regions of strong bright bands correspond to the deep mode. Further research is needed to better understand these two types of stratiform precipitation in monsoonal and ITCZ regions.

The two types of BSRs illustrated by the examples over the Bay of Bengal in Figures 12a and 12b are associated with different large-scale conditions of the monsoon. The vectors in Figure 13 show the 850 hPa wind and height anomalies averaged for times that BSRs occurred during JJA over the Bay of Bengal region shown by the red rectangle in Figure 10b. The anomalies are relative to the JJA climatology. The patterns in Figure 13a are times when robust BSRs, like those in Figures 12a, 12c, 12e, and 12g, were present, while the patterns in Figure 13b are for the times when the weaker, more cellular BSRs, like those in Figures 12b, 12d, 12f, and 12h, were present. These panels show that the more robust cases exhibiting the classic mesoscale convective system structure are associated with a stronger than normal monsoon trough over the northern Bay of Bengal, signaling active periods of the monsoon, when depressions move into the region of the Bay [*Sikka*, 1977; *Shukla*, 1978]. It is known from aircraft radar and microphysics data collected under monsoon depression conditions during the 1979 Monsoon Experiment (MONEX) that mesoscale convective systems with large stratiform regions occur in these depressions [*Houze and Churchill*, 1987]. In contrast, when the weaker, cellular BSRs were present, the height and wind anomalies over the Bay were weak, indicating that this type of BSR was favored in the undisturbed climatological southwest monsoon (as seen in Figure 4b). We further recall from the right-hand panels of Figure 8 that WCC echoes occurring adjacent to
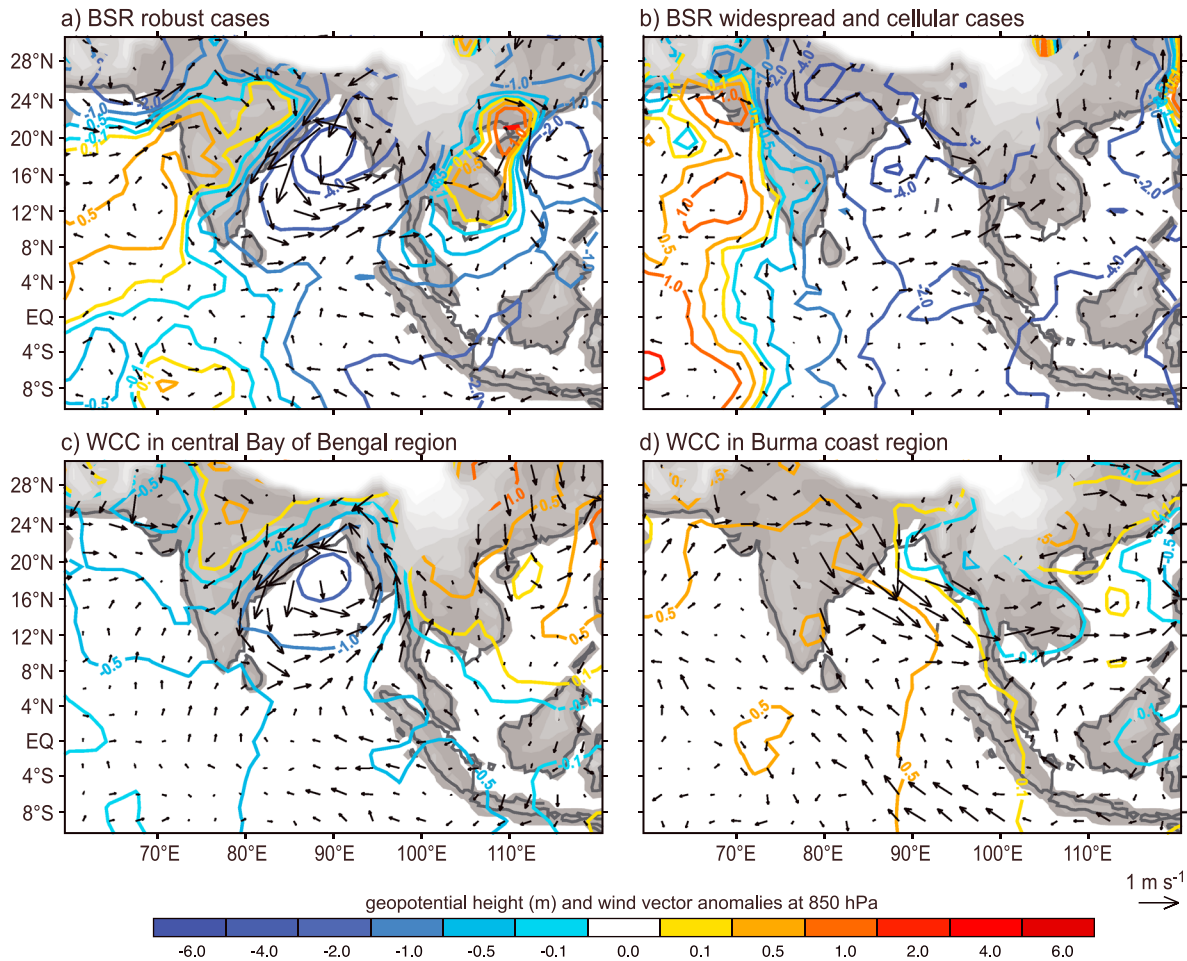
Figure 13. ERA-interim reanalysis composite maps of (a) 850 hPa geopotential height (m) and wind vector anomalies (m s^{-1}) for times of occurrence of (a) BSRs with robust stratiform precipitation and (b) BSRs with widespread and cellular stratiform precipitation. (c and d) Same as Figures 13a and 13b but for WCCs with moderate thresholds in the central Bay of Bengal and Burma coast regions shown in the black boxes in Figure 8b, respectively. The topography is shown in gray shading.

the Burma coast were only those defined by the moderate threshold set (Figure 8b). When we apply the strong thresholds, we see WCCs only over the center of the Bay (Figure 8d). The wind and height anomaly maps in Figures 13c and 13d were computed for times when moderate threshold WCCs occurred in the central Bay of Bengal and Burma Coast regions shown in black boxes in Figure 8b, respectively. The composite map for the western region (central Bay of Bengal) in Figure 13c is similar to the composite for the robust BSR cases shown in Figure 13a, indicating that the WCCs occurring over the central Bay under monsoon depression conditions were precursors to strong mesoscale systems with strong BSRs, such as those observed by *Houze and Churchill* [1987]. The anomaly maps for the BSRs found in the eastern Bay (along the Burma coast) in Figure 13d show no pronounced height anomaly, indicating that they were occurring in more purely southwesterly flow and that the weak cellular but widespread BSRs developed from moderate WCCs piling up along the mountainous coastline in the prevailing southwesterly flow. The somewhat enhanced northwesterly monsoonal flow at 850 hPa seen in Figure 13d is probably related to the monsoon trough being located farther to the north at these times. Note that the magnitude of the anomalous winds is quite small even where enhanced.

7.3. Region of the Plum Rains

An important rainy season in Japan, Korea, southeastern China, and Taiwan that occurs in May–June is referred to in the transliterated languages of the regions as Mei-Yu (Chinese), Tsuyu or Baiu (Japanese), and Jangma (Korean), all of which mean the season of plum rain because the rains coincide with the ripening of plums. This rainy season is actually part of the summer monsoon of eastern Asia. The rainy zone occurs at
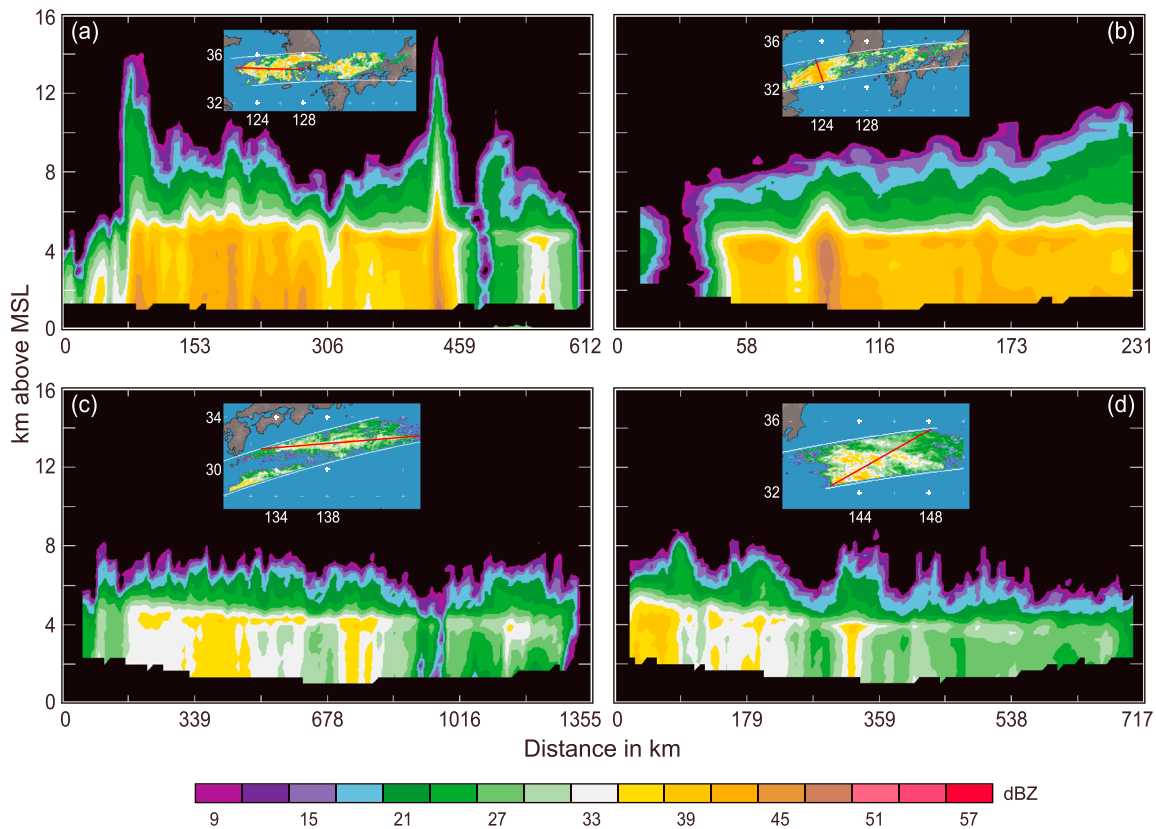
Figure 14. Same as in Figure 11 but for the orange rectangle that represents the plum rain (or Mei-Yu) region shown in Figure 10b. (a and b) Vertical cross sections of TRMM PR data representing robust stratiform precipitation and (c and d) examples of less intense rain with widespread cellular stratiform precipitation and sloping bright bands. Examples of TRMM PR data in the orange region are shown at the following times: 21:02 UTC, 10 July 2010 (Figure 14a), 15:04 UTC, 23 June 2001 (Figure 14b), 02:35 UTC, 5 June 2012 (Figure 14c), and 00:13 UTC, 3 June 2008 (Figure 14d).

the northeastern extremity of the southwest flow emerging from the monsoonal low over South Asia. Convergence of monsoonal moisture flux in this wind regime results in maximum rainfall occurring in a southwest-northeast band extending across the South China Sea. This band of rainfall migrates northward as the monsoon season progresses affecting southeastern China and Taiwan at first and later Korea and southern Japan. This belt is colloquially known as the Mei-Yu, Baiu, or Jangma "front"; however, it is not a front in the usual sense, but rather just an elongated area of maximum climatological rainfall. *Ninomiya and Mizuno* [1987], *Ninomiya and Akiyama* [1992], and *Chen* [1994] describe the large-scale circulation pattern producing this rain area. The plum rain maximum is seasonally forced by the Asian monsoon; however, it undergoes intraseasonal variations connected with transitory midlatitude troughs and ridges to the north. The TRMM PR data obtained in the plum rain regime exhibit behaviors somewhat like the precipitation systems seen over the Bay of Bengal and other monsoonal regions. The examples in Figures 14a and 14b are similar to those seen in Figures 12a, 12c, 12e, and 12g. The less robust examples in Figures 14c and 14d (both from the early June plum rain season), on the other hand, are only partially similar to the less robust examples in Figures 12b, 12d, 12f, and 12h. The difference is that the examples in the plum rain region sometimes exhibit sloping bright bands, indicating that this region near the northern edge of the TRMM domain sometimes has a baroclinic aspect that could be affecting the precipitation forming processes. This possibility needs detailed examination.

7.4. Frontal Zones

Stratiform precipitation occurs near the subtropical extremities of the TRMM swath as a result of frontal systems, not convective systems. These stratiform precipitation regions are often large enough to be detected by the TRMM PR algorithm as BSRs; indeed, they are on average much larger than the BSRs of lower latitudes, a further indication of their frontal nature. These stratiform regions are usually easily distinguishable from the
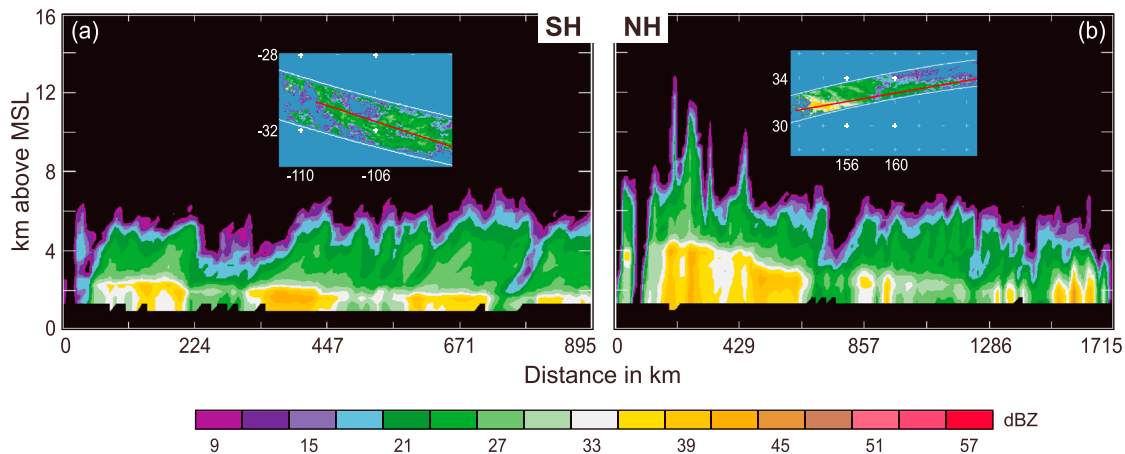
Figure 15. Same as in Figure 11 but for the green rectangles that represent the midlatitude frontal regions shown in Figure 10. A vertical cross section of TRMM PR data representing a very low and sloping bright band feature is shown at (a) 10:22 UTC, 15 July 2012 from the green rectangle in the South Pacific region (Figure 10d). A vertical cross section of TRMM PR data representing a steeply sloping bright band is shown at (b) 23:56 UTC, 13 January 2001 in the North Pacific region (Figure 10a).

stratiform regions characteristic of deep convective precipitation in the equatorial regions. For example, *Viale et al.* [2013] used TRMM radar data of a frontal stratiform region to test model output for an "atmospheric river" frontal system intersecting the Andes. Because of the cooler and baroclinic conditions in frontal systems, the bright band signifying the melting layer in these frontal cases is at an altitude well below the nearly constant level of ~5 km in the tropics, and often the bright band slopes as a result of the temperature gradient. The BSRs in these subtropical zones in winter almost all have the quality of low and/or sloping bright bands. The example cross section in Figure 15a slopes downward from a height of ~2 km down to ~1 km over horizontal distance of about 700 km, while the example in Figure 15b slopes from 4 km sharply down to about 2 km over a distance of ~200 km.

8. Conclusions

The TRMM satellite was designed to document climatologically the global pattern of rainfall and latent heat release at lower latitudes. The novel precipitation-measuring radar aboard the satellite was a key part of the instrument suite to accomplish this goal. An additional benefit of having a radar in space and collecting data for over 16 years has been the documentation of the vertical structures of radar echoes producing rainfall over the tropics and subtropics. Precipitation radars have long been the most important instruments for determining the nature of convective systems. The benefit of spaceborne radar is to be able to compare the nature of convective systems across the entire domain of the tropics and subtropics. This paper summarizes much of what we have learned from such comparisons.

The TRMM PR was not a highly sophisticated radar system. It detected only reflectivity. It had no ability to extract Doppler velocity, dual-polarimetric comparisons, or multiwavelength information. It had a low sensitivity of only 17 dBZ, and because of the orbital characteristics, obtained only snapshots ~2 times a day at most locations. Nevertheless, when vertical profiles of the three-dimensional data from these snapshots are processed and examined in detail, it is possible to distinguish convective and stratiform echoes, determine the juxtaposition of these features, measure their spatial dimensions, and see their intensities and general characteristics. By compiling this information, deriving metrics of the echoes based on their three-dimensional structures, and mapping these metrics over the entirety of the tropics and subtropics, we have been able to see how the nature of convection varies across low latitudes. By interpolating the data to Cartesian coordinates, we have been able to further examine a large quantity of the TRMM PR data with visualization software of the type used to analyze radar data from ordinary ground, ship, and aircraft platforms to yield further insight into the nature of the convection producing the rainfall.

One prominent result is the finding that isolated shallow convection (ISEs) is an almost entirely oceanic phenomenon, while extremely deep and intense convection (DCCs identified by the strong threshold set) is nearly exclusively an over-land phenomenon. The deep, intense convection over land, moreover, tends

to occur in more arid regions, especially near, but not over, the high mountains of the Himalayas and Andes. DCCs defined by more relaxed (moderate) thresholds do occur over the oceans.

Much, but not all, tropical and subtropical precipitation can be thought of as being in different life cycle stages of mesoscale convective systems of the type reviewed by *Houze* [2004, 2014, Chapter 9]. The three-dimensional echo elements that we have identified as wide convective cores (WCCs) represent intense convective echoes that are embedded in cloud systems that have grown upscale into mesoscale systems, as suggested by *Romatschke and Houze* [2010] and demonstrated by *Zuluaga and Houze* [2013]. Over the landmasses of central equatorial Africa and subtropical South America, extremely intense convection (with DCCs identified by the strong threshold set) evolves frequently into mesoscale systems containing the widest and most intense convection (i.e., containing WCCs identified by strong thresholds). Although the occurrence of these most extreme manifestations of convection concentrates in these regions, these areas are not the areas of most rainfall in the tropics and subtropics.

In both DJF and JJA, rainfall maximizes over oceanic ITCZ regions, the Amazon, and the Maritime continent. Over these rainy zones, mesoscale system occurrence is frequent. However, the convective elements and mesoscale systems in these regions are mostly of a more moderate nature (convective clouds with moderate DCCs growing into mesoscale systems containing moderate WCCs). In JJA, additional convective behaviors occur in the South Asian monsoon and Mesoamerican zones, when mesoscale systems containing moderate threshold WCCs concentrate along coastlines, especially where mountains line the coasts and the low-level winds are persistently onshore. These mesoscale systems develop from convection with moderate threshold convective cores. Over the Bay of Bengal, a secondary maximum of occurrence of mesoscale systems with WCCs occurs over the central Bay of Bengal, and many of these are more intense (containing WCCs defined by strong thresholds). These stronger threshold mesoscale systems, however, develop from cloud systems containing only moderate convection (containing DCCs defined by moderate thresholds).

As mesoscale convective systems age, they often develop attendant regions of stratiform precipitation, consisting of previously active convective cloud [*Houze*, 1997, 2014, Chapter 6]. In this study, we have determined the frequency of occurrence of very large areas of stratiform precipitation (BSRs). These statistics show that BSRs occur most frequently over ocean and that there are different types of BSRs, some probably not associated with mesoscale convective systems of the type described by *Houze* [2004] and *Houze* [2014, Chapter 9]. This fact cautions against assuming that all stratiform precipitation seen by TRMM (or GPM) in the tropics and subtropics has a canonical profile of latent heating of the type seen in mesoscale convective systems. In ITCZ regions and monsoonal regions upwind of coastlines, many of the BSRs have the form of widespread regions of weak-to-moderate precipitation with numerous embedded convective cells. The vertical air motions in these regions are sufficiently weak to allow a faint bright band to extend across the region rendering the echo to appear stratiform according to the method of *Awaka et al.* [1997], which is the primary factor used to identify stratiform precipitation for TRMM product 2A23. Hence, these areas are identified (possibly incorrectly) as BSRs. The weakening of a previously more active mesoscale region of more intense convection could form these features, or they could be simply weak convection congregated into a single large area. The latter scenario seems more likely since this type of BSR occurs most frequently where persistent onshore winds converge upstream of coastal mountains, especially on the Burma coast during the South Asian monsoon. In regions where fronts extend into the subtropics, the BSRs take on yet another form. They have structures somewhat like the cellular BSRs in ITCZ and monsoon regions, but in addition have bright bands that are often much lower than the ~5 km level of the tropical 0°C level and frequently are seen to slope downward toward colder regions, reflecting their origin in regions of baroclinic upward motions. BSRs in the late spring "plum rain" region of southeastern Asia form where the southwesterly monsoon flow emanating from the Indian monsoonal region converges near Japan. The BSRs in this region have a variety of structures, including strong coherent mesoscale system stratiform areas, widespread weak cellular BSRs, and BSRs with sloping bright bands. This mix of BSR structures is consistent with the prevailing southwest monsoon being intermittently interrupted by midlatitude baroclinic waves.

Thus, the statistics of 16 years of TRMM PR data have shown that stratiform precipitation varies in its nature across the tropics and subtropics. Because the TRMM latent heating algorithm products 2H25 and CSH are based on models representing robust tropical MCSs, one should exercise caution in applying these heating profiles to all stratiform precipitation in the TRMM data set. One important type of precipitating system that is not highlighted in the statistics of this study is the clouds of tropical cyclones, which are not numerous enough to

affect the conclusions of this study. However, in other studies, *Hence and Houze* [2011, 2012a, 2012b] have extracted the TRMM PR samples of tropical cyclones over the Atlantic and Pacific bases and examined the vertical structures of both eyewall and rainband precipitation. They found that the eyewall and rainband clouds have regions of precipitation exhibiting robust bright bands. These rainfall regions may have profiles of latent heating somewhat similar to mesoscale convective systems in nonrotating environments, but likely these profiles also differ in some respects as a result of the completely different dynamics at play. Therefore, it seems advisable to estimate the heating profiles in tropical cyclones with models of tropical cyclone cloud systems rather than 2H25 and CSH. Given the variety of forms of stratiform precipitation seen in vertical cross sections of TRMM PR data, perhaps the TRMM latent heating algorithms need some modification.

Possibly the most important result of the evaluation of the variable nature of convection across the tropics and subtropics described in this paper is that deep convection cannot be viewed as a single kind of entity. As the global climate changes, patterns of deep convection in all its forms may change, and such changes can be determined only if models can forecast the variable nature of convection in a wide range of ocean, land, island, coastal, and mountain regimes. Parameterization methods that treat all deep convection the same way cannot account for this variability. Global and regional models of the future will therefore need to account explicitly for the occurrence of convection with moderate and strong convective and mesoscale features and for different types of associated stratiform precipitation.

Glossary of Acronyms

2A23	TRMM PR rain characteristics data set. It includes the separation of the PR-observed rain into convective, stratiform, and other categories.
2A25	TRMM PR precipitation echo data set. It includes the attenuation corrected radar reflectivity along the slant range of the scanning radar beam and related parameters.
2H25	TRMM PR Spectral Latent Heating data set. This field provides latent heating rate along the slant range of the radar computed from radar-estimated convective and stratiform rain amounts and other characteristics of the PR radar echo field. The method is based on *Shige et al.* [2004, 2007, 2008, 2009].
2H31	TRMM PR Convective-Stratiform Heating data set. provides latent heating rate along the slant range of the radar computed from radar-estimated convective and stratiform rain amounts and other characteristics of the PR radar echo field. The method is described by *Tao et al.* [1993, 2000, 2001, 2010, 2015].
BSR	Broad stratiform region—a contiguous stratiform echo covering at least 40,000 km^2 (moderate threshold) or 50,000 km^2 (strong threshold).
CaPE	Convection and Precipitation/Electrification Experiment
DCC	Deep convective core—a contiguous three-dimensional convective echo object exceeding either the moderate or strong threshold intensity whose tops exceed a height threshold. For echo objects defined by the moderate threshold intensity of 30 dBZ, the echo objects' top-height threshold is 8 km to qualify as a DCC; for the strong threshold intensity of 40 dBZ, the height threshold is 10 km.
DJF	December-January-February
DRA	Distinguishable rain area
GPM	Global Precipitation Measurement Mission
ISE	Isolated shallow echo—a precipitating element seen on radar whose echo top is at least 1 km below the 0°C level and may be thought of as showers of "warm rain."
ITCZ	Intertropical Convergence Zone
JJA	June-July-August
MCS	Mesoscale convective system
MONEX	1979 Monsoon Experiment
NAME	North American Monsoon Experiment
PR TRMM	Ku-band precipitation radar
TOGA COARE	Tropical Ocean Global Atmosphere Coupled Ocean Atmosphere Response Experiment
TRMM	Tropical Rainfall Measuring Mission

References

Adler, R. F., G. J. Huffman, D. T. Bolvin, S. Curtis, and E. J. Nelkin (2000), Tropical rainfall distribution determined using TRMM combined with other satellite and rain gauge information, *J. Appl. Meteorol.*, *39*, 2007–2023.

Arakawa, A., and W. H. Schubert (1974), Interaction of a cumulus ensemble with the large-scale environment: Part I, *J. Atmos. Sci.*, *31*, 674–701.

Awaka J., T. Iguchi, H. Kumagai, and K. Okamoto (1997), Rain type classification algorithm for TRMM Precipitation Radar, in *Geoscience and Remote Sensing, 1997: IGARSS '97, Remote Sensing—A Scientific Vision for Sustainable Development*, vol. 4, pp. 1633–1635, Institute of Electrical and Electronics Engineers, New York, doi:10.1109/IGARSS.1997.608993.

Barnes, H. C., and R. A. Houze Jr. (2013), The precipitating cloud population of the Madden-Julian Oscillation over the Indian and West Pacific Oceans, *J. Geophys. Res. Atmos.*, *118*, 6996–7023, doi:10.1002/jgrd.50375.

Barnes, H. C., M. D. Zuluaga, and R. A. Houze Jr. (2015), Latent heating characteristics of the MJO computed from TRMM observations, *J. Geophys. Res. Atmos.*, *120*, 1322–1334, doi:10.1002/2014JD022530.

Barros, A. P., G. Kim, E. Williams, and S. W. Nesbitt (2004), Probing orographic controls in the Himalayas during the monsoon using satellite imagery, *Nat. Hazards Earth Syst. Sci.*, *4*, 29–51.

Biasutti, M., S. E. Yuter, C. D. Burleyson, and A. H. Sobel (2012), Very high resolution rainfall patterns measured by TRMM Precipitation Radar: Seasonal and diurnal cycles, *Clim. Dyn.*, *39*, 239–258.

Boccippio, D. J., W. A. Petersen, and D. J. Cecil (2005), The tropical convective spectrum. Part I: Archetypal vertical structures, *J. Clim.*, *18*, 2744–2769.

Bosart, L. F., and F. Sanders (1981), The Johnstown flood of July 1977: A long-lived convective system, *J. Atmos. Sci.*, *38*, 1616–1642.

Burpee, R. W., and L. N. Lahiff (1984), Area-average rainfall variations on sea-breeze days in south Florida, *Mon. Weather Rev.*, *112*, 520–534.

Chen, G. T.-J. (1994), Large-scale circulations associated with the East Asian summer monsoon and the Mei-Yu over South China and Taiwan, *J. Meteorol. Soc. Jpn.*, *72*, 959–983.

Chen, S. S., R. A. Houze Jr., and B. E. Mapes (1996), Multiscale variability of deep convection in relation to large-scale circulation in TOGA COARE, *J. Atmos. Sci.*, *53*, 1380–1409.

Cifelli, R., W. A. Petersen, L. D. Carey, S. A. Rutledge, and M. A. F. da Silva Dias (2002), Radar observations of the kinematic, microphysical, and precipitation characteristics of two MCSs in TRMM LBA, *J. Geophys. Res.*, *107*(D20), 8077, doi:10.1029/2000JD000264.

Corbet, J., C. Mueller, C. Burghart, K. Gould, and G. Granger (1994), Zeb: Software for geophysical data integration, display, and management of diverse environmental datasets, *Bull. Am. Meteorol. Soc.*, *75*, 783–792.

DeMott, C. A., and S. A. Rutledge (1998), The vertical structure of TOGA COARE convection. Part II: Modulating influences and implications for diabatic heating, *J. Atmos. Sci.*, *55*, 2748–2762.

Douglas, M. W. (1992a), Structure and dynamics of two monsoon depressions. Part I: Observed structure, *Mon. Weather Rev.*, *120*, 1524–1547.

Douglas, M. W. (1992b), Structure and dynamics of two monsoon depressions. Part II: Vorticity and heat budgets, *Mon. Weather Rev.*, *120*, 1548–1564.

Emanuel, K., A. A. Wing, and E. M. Vincent (2014), Radiative-convective instability, *J. Adv. Model. Earth Syst.*, *6*, 75–90, doi:10.1002/2013MS000270.

Fritsch, J. M., J. D. Murphy, and J. S. Kain (1994), Warm core vortex amplification over land, *J. Atmos. Sci.*, *51*, 1781–1806.

Funk, A., C. Schumacher, and J. Awaka (2013), Analysis of rain classifications over the tropics by Version 7 of the TRMM PR 2A23 algorithm, *J. Meteorol. Soc. Jpn.*, *91*, 257–272, doi:10.2151/jmsj.2013-302.

Godbole, R. V. (1977), The composite structure of the monsoon depression, *Tellus*, *29*, 25–40.

Hager, W. W., R. G. Sonnenfeld, W. Feng, T. Kanmae, H. C. Stenbaek-Nielsen, M. G. McHarg, R. K. Haaland, S. A. Cummer, G. Lu, and J. L. Lapierre (2012), Charge rearrangement by sprites over a north Texas mesoscale convective system, *J. Geophys. Res.*, *117*, D22101, doi:10.1029/2012JD018309.

Hartmann, D. L., H. H. Hendon, and R. A. Houze Jr. (1984), Some implications of the mesoscale circulations in tropical cloud clusters for large-scale dynamics and climate, *J. Atmos. Sci.*, *41*, 113–121.

Hence, D. A., and R. A. Houze Jr. (2011), Vertical structure of hurricane eyewalls as seen by the TRMM Precipitation Radar, *J. Atmos. Sci.*, *68*, 1637–1652.

Hence, D. A., and R. A. Houze Jr. (2012a), Vertical structure of tropical cyclones with concentric eyewalls as seen by the TRMM Precipitation Radar, *J. Atmos. Sci.*, *69*, 1021–1036.

Hence, D. A., and R. A. Houze Jr. (2012b), Vertical structure of tropical cyclone rainbands as seen by the TRMM Precipitation Radar, *J. Atmos. Sci.*, *69*, 2644–2661.

Higgins, W., et al. (2006), The NAME 2004 field campaign and modeling strategy, *Bull. Am. Meteorol. Soc.*, *87*, 79–94, doi:10.1175/BAMS-87-1-79.

Hou, A. Y., R. K. Kakar, S. Neeck, A. A. Azarbarzin, C. D. Kummerow, M. Kojima, R. Oki, K. Nakamura, and T. Iguchi (2014), The global precipitation measurement mission, *Bull. Am. Meteorol. Soc.*, *95*, 701–722, doi:10.1175/BAMS-D-13-00164.1.

Houze, R. A., Jr. (1982), Cloud clusters and large-scale vertical motions in the tropics, *J. Meteorol. Soc. Jpn.*, *60*, 396–410.

Houze, R. A., Jr. (1989), Observed structure of mesoscale convective systems and implications for large-scale heating, *Q. J. R. Meteorol. Soc.*, *115*, 425–461.

Houze, R. A., Jr. (1997), Stratiform precipitation in regions of convection: A meteorological paradox?, *Bull. Am. Meteorol. Soc.*, *78*, 2179–2196.

Houze, R. A., Jr. (2004), Mesoscale convective systems, *Rev. Geophys.*, *42*, RG4003, doi:10.1029/2004RG000150.

Houze, R. A., Jr. (2014), *Cloud Dynamics*, 2nd ed., 432 pp., Elsevier/Academic Press, Oxford.

Houze, R. A., Jr., and D. D. Churchill (1987), Mesoscale organization and cloud microphysics in a Bay of Bengal depression, *J. Atmos. Sci.*, *44*, 1845–1868.

Houze, R. A., Jr., B. F. Smull, and P. Dodge (1990), Mesoscale organization of springtime rainstorms in Oklahoma, *Mon. Weather Rev.*, *118*, 613–654.

Houze, R. A., Jr., S. S. Chen, D. E. Kingsmill, Y. Serra, and S. E. Yuter (2000), Convection over the Pacific warm pool in relation to the atmospheric Kelvin-Rossby wave, *J. Atmos. Sci.*, *57*, 3058–3089.

Houze, R. A., Jr., D. C. Wilton, and B. F. Smull (2007), Monsoon convection in the Himalayan region as seen by the TRMM Precipitation Radar, *Q. J. R. Meteorol. Soc.*, *133*, 1389–1411.

Houze, R. A., Jr., W.-C. Lee, and M. M. Bell (2009), Convective contribution to the genesis of Hurricane Ophelia, 2005, *Mon. Weather Rev.*, *137*, 2778–2800.

Hoxit, L. R., C. F. Chappell, and J. M. Fritsch (1976), Formation of mesolows or pressure troughs in advance of cumulonimbus clouds, *Mon. Weather Rev.*, *104*, 1419–1428.

Huffman, G. J., R. F. Adler, D. T. Bolvin, G. Gu, E. J. Nelkin, K. P. Bowman, E. F. Stocker, and D. B. Wolff (2007), The TRMM Multi-satellite precipitation analysis: Quasi-global, multi-year, combined-sensor precipitation estimates at fine scale, *J. Hydrometeorol.*, *8*, 33–55.

James, C. N., S. R. Brodzik, H. Edmon, R. A. Houze Jr., and S. E. Yuter (2000), Radar data processing and visualization over complex terrain, *Weather Forecasting*, *15*, 327–338.

Johnson, R. H., and R. A. Houze Jr. (1987), Precipitating cloud systems of the Asian monsoon, in *Monsoon Meteorology*, edited by C.-P. Chang and T. N. Krishnamurti, pp. 298–353, Oxford Univ. Press, Oxford.

Kingsmill, D. E., and R. A. Houze Jr. (1999), Kinematic characteristics of air flowing into and out of precipitating convection over the west Pacific warm pool: An airborne Doppler radar survey, *Q. J. R. Meteorol. Soc.*, *125*, 1165–1207.

Krishnamurti, T. N. (1985), Summer monsoon experiment—A review, *Mon. Weather Rev.*, *113*, 1590–1626.

Krishnamurti, T. N., M. Kanamitsu, R. Godbole, C.-B. Chang, F. Carr, and J. H. Chow (1975), Study of a monsoon depression (I): Synoptic structure, *J. Meteorol. Soc. Jpn.*, *53*, 227–239.

Kummerow, C., W. Barnes, T. Kozu, J. Shiue, and J. Simpson (1998), The Tropical Rainfall Measuring Mission (TRMM) sensor package, *J. Atmos. Oceanic Technol.*, *15*, 809–817.

Kummerow, C., et al. (2000), The status of the Tropical Rainfall Measuring Mission (TRMM) after two years in orbit, *J. Appl. Meteorol.*, *39*, 1965–1982.

LeMone, M. A., and E. J. Zipser (1980), Cumulonimbus vertical velocity events in GATE. Part I: Diameter, intensity, and mass flux, *J. Atmos. Sci.*, *37*, 2444–2457.

Liu, C. (2011), Rainfall contribution from precipitation systems with different sizes, intensities and durations, *J. Hydrometeorol.*, *12*, 394–412.

Liu, C., and E. J. Zipser (2005), Global distribution of convection penetrating the tropical tropopause, *J. Geophys. Res.*, *110*, D23104, doi:10.1029/2005JD00006063.

Liu, C., and E. J. Zipser (2008), Diurnal cycles of precipitation, clouds, and lightning in the tropics from 9 years of TRMM observations, *Geophys. Res. Letters*, *35*, L04819, doi:10.1029/2007GL032437.

Liu, C., and E. J. Zipser (2009), "Warm rain" in the tropics: Seasonal and regional distribution based on 9 years of TRMM data, *J. Clim.*, *22*, 767–779, doi:10.1175/2008JCLI2641.1.

Liu, C., E. J. Zipser, D. J. Cecil, S. W. Nesbitt, and S. Sherwood (2008), A cloud and precipitation feature database from 9 years of TRMM observations, *J. Appl. Meteorol. Climatol.*, *47*, 2712–2728, doi:10.1175/2008JAMC1890.1.

Liu, C., E. Williams, E. J. Zipser, and G. Burns (2010), Diurnal variations of global thunderstorms and electrified shower clouds and their contribution to the global electrical circuit, *J. Atmos. Sci.*, *67*, 309–323.

Liu, C., D. Cecil, and E. J. Zipser (2012), Relationships between lightning flash rates and radar reflectivity vertical structures in thunderstorms over the tropics and subtropics, *J. Geophys. Res.*, *117*, D06212, doi:10.1029/2011JD017123.

Liu, C., S. Shige, Y. N. Takayabu, and E. Zipser (2015), Latent heating contribution from precipitation systems with different sizes, depths, and intensities in the tropics, *J. Clim.*, *28*, 186–203.

Mapes, B. E., and R. A. Houze Jr. (1993), Cloud clusters and superclusters over the oceanic warm pool, *Mon. Weather Rev.*, *121*, 1398–1415.

Medina, S., R. A. Houze Jr., A. Kumar, and D. Niyogi (2010), Summer monsoon convection in the Himalayan region: Terrain and land cover effects, *Q. J. R. Meteorol. Soc.*, *136*, 593–616.

Moncrieff, M. W. (1992), Organized convective systems: Archetypical dynamical models, mass and momentum flux theory, and parameterization, *Q. J. R. Meteorol. Soc.*, *118*, 819–850.

Nakazawa, T. (1988), Tropical super clusters within intraseasonal variations over the western Pacific, *J. Meteorol. Soc. Jpn.*, *66*, 823–839.

Nesbitt, S., and A. Anders (2009), Very high resolution climatologies from the Tropical Rainfall Measuring Mission Precipitation Radar, *Geophys. Res. Lett.*, *36*, L15815, doi:10.1029/2009GL038026.

Nesbitt, S. W., E. J. Zipser, and D. J. Cecil (2000), A census of precipitation features in the tropics using TRMM: Radar, ice scattering, and ice observations, *J. Clim.*, *13*, 4087–4106.

Ninomiya, K., and T. Akiyama (1992), Multi-scale features of Baiu, the summer monsoon over Japan and the East Asia, *J. Meteorol. Soc. Jpn.*, *70*, 467–495.

Ninomiya, K., and H. Mizuno (1987), Variations of Baiu precipitation over Japan in 1951–1980 and large-scale characteristics of wet and dry Baiu, *J. Meteorol. Soc. Jpn.*, *65*, 115–127.

Pandya, R., and D. Durran (1996), The influence of convectively generated thermal forcing on the mesoscale circulation around squall lines, *J. Atmos. Sci.*, *53*, 2924–2951.

Ramage, C. S. (1968), Role of a tropical "maritime continent" in the atmospheric circulation, *Mon. Weather Rev.*, *96*, 365–370.

Ramage, C. S. (1971), *Monsoon Meteorology*, 271 pp., Academic Press, New York.

Rao, Y. P. (1976), *Southwest Monsoon, Meteorol. Monograph. Synoptic Meteorol. No. 1/1976*, 367 pp., Indian Department of Meteorology, New Delhi.

Rasmussen, K. L., and R. A. Houze Jr. (2011), Orogenic convection in South America as seen by the TRMM satellite, *Mon. Weather Rev.*, *139*, 2399–2420.

Rasmussen, K. L., M. D. Zuluaga, and R. A. Houze Jr. (2014), Severe convection and lightning in subtropical South America, *Geophys. Res. Lett.*, *41*, 7359–7366, doi:10.1002/2014GL061767.

Rickenbach, T. M., and S. A. Rutledge (1998), Convection in TOGA COARE: Horizontal scale, morphology, and rainfall production, *J. Atmos. Sci.*, *55*, 2715–2729.

Romatschke, U., and R. A. Houze Jr. (2010), Extreme summer convection in South America, *J. Clim.*, *23*, 3761–3791.

Romatschke, U., and R. A. Houze Jr. (2013), Characteristics of precipitating convective systems accounting for the summer rainfall of tropical and subtropical South America, *J. Hydrometeorol.*, *14*, 25–46.

Romatschke, U., S. Medina, and R. A. Houze Jr. (2010), Regional, seasonal, and diurnal variations of extreme convection in the South Asian region, *J. Clim.*, *23*, 419–439.

Rowe, A. K., S. A. Rutledge, T. J. Lang, P. E. Ciesielski, and S. M. Saleeby (2008), Elevation-dependent trends in precipitation observed during NAME, *Mon. Weather Rev.*, *136*, 4962–4979.

Rowe, A. K., S. A. Rutledge, and T. J. Lang (2011), Investigation of microphysical processes occurring in isolated convection during NAME, *Mon. Weather Rev.*, *139*, 2168–2187.

Rowe, A. K., S. A. Rutledge, and T. J. Lang (2012), Investigation of microphysical processes occurring in organized convection during NAME, *Mon. Weather Rev.*, *140*, 424–443.

Sanders, F. (1984), Quasi-geostrophic diagnosis of the monsoon depression of 5–8 July, 1979, *J. Atmos. Sci.*, *41*, 538–552.

Sawyer, J. S. (1947), The structure of the intertropical front over N.W. India during the S.W. monsoon, *Q. J. R. Meteorol. Soc.*, *73*, 346–369.

Schumacher, C., and R. A. Houze Jr. (2003a), Stratiform rain in the tropics as seen by the TRMM Precipitation Radar, *J. Clim.*, *16*, 1739–1756.

Schumacher, C., and R. A. Houze Jr. (2003b), The TRMM Precipitation Radar's view of shallow, isolated rain, *J. Appl. Meteorol.*, *42*, 1519–1524.

Schumacher, C., R. A. Houze Jr., and I. Kraucunas (2004), The tropical dynamical response to latent heating estimates derived from the TRMM Precipitation Radar, *J. Atmos. Sci.*, *61*, 1341–1358.

Shige, S., Y. N. Takayabu, W.-K. Tao, and D. E. Johnson (2004), Spectral retrieval of latent heating profiles from TRMM PR data. Part I: Development of a model-based algorithm, *J. Appl Meteorol.*, *43*, 1095–1113.

Shige, S., Y. N. Takayabu, W.-K. Tao, and C. L. Shie (2007), Spectral retrieval of latent heating profiles from TRMM PR data. Part II: Algorithm improvement and heating estimates over tropical ocean regions, *J. Appl. Meteorol.*, *46*, 1098–1124.

Shige, S., Y. N. Takayabu, and W.-K. Tao (2008), Spectral retrieved of latent heating profiles from TRMM PR data. Part III: Moistening estimates over the tropical ocean regions, *J. Appl. Meteorol. Climatol.*, *47*, 620–640.

Shige, S., Y. N. Takayabu, S. Kida, W.-K. Tao, X. Zeng, and T. L'Ecuyer (2009), Spectral retrieved of latent heating profiles from TRMM PR data. Part IV: Comparisons of lookup tables from two- and three-dimensional simulations, *J. Clim.*, *22*, 5577–5594.

Short, D. A., and K. Nakamura (2010), Effect of TRMM orbital boost on radar reflectivity distributions, *J. Atmos. Oceanic Technol.*, *27*, 1247–1254.

Shukla, J. (1978), CISK-barotropic-baroclinic instability and the growth of monsoon depressions, *J. Atmos. Sci.*, *35*, 495–508.

Sikka, D. R. (1977), Some aspects of the life history, structure and movement of monsoon depressions, *Pure Appl. Geophys.*, *115*, 1501–1529.

Simpson, J., R. F. Adler, and G. R. North (1988), A proposed Tropical Rainfall Measuring Mission (TRMM) satellite, *Bull. Am. Meteorol. Soc.*, *69*, 278–295.

Tao, W.-K., S. Lang, J. Simpson, and R. Adler (1993), Retrieval algorithms for estimating the vertical profiles of latent heat release: Their applications for TRMM, *J. Meteorol. Soc. Jpn.*, *71*, 685–700.

Tao, W.-K., S. Lang, J. Simpson, W. S. Olson, D. Johnson, B. Ferrier, C. Kummerow, and R. Adler (2000), Retrieving vertical profiles of latent heat release in TOGA COARE convective systems using a cloud resolving model, SSM/I and radar data, *J. Meteorol. Soc. Jpn.*, *78*, 333–355.

Tao, W.-K., S. Lang, W. S. Olson, R. Meneghini, S. Yang, J. Simpson, C. Kummerow, E. Smith, and J. Halverson (2001), Retrieved vertical profiles of latent heat release using TRMM rainfall products for February 1998, *J. Appl. Meteorol.*, *40*, 957–982.

Tao, W.-K., et al. (2006), Retrieval of latent heating from TRMM measurements, *Bull. Am. Meteorol. Soc.*, *87*, 1555–1572.

Tao, W.-K., R. A. Houze Jr., and E. A. Smith (2007), The fourth TRMM latent heating workshop, *Bull. Am. Meteorol. Soc.*, *88*, 1255–1259.

Tao, W.-K., S. Lang, X. Zeng, S. Shige, and Y. Takayabu (2010), Relating convective and stratiform rain to latent heating, *J. Clim.*, *23*, 1874–1893.

Tao, W.-K., et al. (2015), TRMM latent heating retrieval: Applications and comparisons with field campaigns and large-scale analyses, *Meteorol. Monogr.*, in press.

Toracinta, E. R., D. J. Cecil, E. J. Zipser, and S. W. Nesbitt (2002), Radar, passive microwave, and lightning characteristics of precipitating systems in the tropics, *Mon. Weather Rev.*, *130*(4), 802–824.

Viale, M., R. A. Houze Jr., and K. L. Rasmussen (2013), Upstream orographic enhancement of a narrow cold-frontal rainband approaching the Andes, *Mon. Weather Rev.*, *141*, 1708–1730.

Wing, A. A., and K. A. Emanuel (2013), Physical mechanisms controlling self-aggregation of convection in idealized numerical modeling simulations, *J. Adv. Model. Earth. Syst.*, *5*, doi:10.1002/2013MS000269.

Xu, K.-M., and K. A. Emanuel (1989), Is the tropical atmosphere conditionally unstable?, *Mon. Weather Rev.*, *117*, 1471–1479.

Yuter, S. E., and R. A. Houze Jr. (1995a), Three-dimensional kinematic and microphysical evolution of Florida cumulonimbus. Part I: Spatial distribution of updrafts, downdrafts, and precipitation, *Mon. Weather Rev.*, *123*, 1921–1940.

Yuter, S. E., and R. A. Houze Jr. (1995b), Three-dimensional kinematic and microphysical evolution of Florida cumulonimbus. Part II: Frequency distribution of vertical velocity, reflectivity, and differential reflectivity, *Mon. Weather Rev.*, *123*, 1941–1963.

Yuter, S. E., and R. A. Houze Jr. (1995c), Three-dimensional kinematic and microphysical evolution of Florida cumulonimbus. Part III: Vertical mass transport, mass divergence, and synthesis, *Mon. Weather Rev.*, *123*, 1964–1983.

Zhang, C., M. McGauley, and N. A. Bond (2004), Shallow meridional circulation in the tropical eastern Pacific, *J. Clim.*, *17*, 133–139.

Zipser, E. J., and C. Gautier (1978), Mesoscale events within a GATE tropical depression, *Mon. Weather Rev.*, *106*, 789–805.

Zipser, E. J., and M. A. LeMone (1980), Cumulonimbus vertical velocity events in GATE. Part II: Synthesis and model core structure, *J. Atmos. Sci.*, *37*, 2458–2469.

Zipser, E. J., D. J. Cecil, C. Liu, S. W. Nesbitt, and D. P. Yorty (2006), Where are the most intense thunderstorms on Earth?, *Bull. Am. Meteorol. Soc.*, *87*, 1057–1071.

Zuluaga, M. D., and R. A. Houze Jr. (2013), Evolution of the population of precipitating convective systems over the Equatorial Indian Ocean in active phases of the Madden-Julian Oscillation, *J. Atmos. Sci.*, *70*, 2713–2725.

Zuluaga, M. D., and R. A. Houze Jr. (2015), Extreme convection of the near-equatorial Americas, Africa, and adjoining oceans as seen by TRMM, *Mon. Weather Rev.*, *143*, 298–316.

Zuluaga, M. D., C. D. Hoyos, and P. J. Webster (2010), Spatial and temporal distribution of latent heating in the South Asian monsoon region, *J. Clim.*, *23*, 2010–2029.